Short guide for resistivity and induced polarization tomography

Short guide for resistivity tomography

This guide brings a brief description of geophysical and technical features of the resistivity tomography accompanied with illustrative examples of measured resistivity sections. This new edition is completed by theoretical derivation of depth sensitivities of all basic measuring arrays. You can find this chapter at the end of the brochure.

Chapter 1
Comparison of main measuring arrays

Illustrative comparison of features of the main measuring arrays used for the resistivity tomography will be shown in this chapter. This short overview can help with the choice of optimum solution with the respect to the studied problem.

Schlumberger

Purpose
General purpose array covering broad range of tasks - especially imaging of horizontal and quasi-horizontal (declined) layers. Detection of larger inhomogeneity of various shape and direction like wider crackles, tectonic zones, ore veins and contacts of layers with big difference of resistivity is also effective.

Section coverage
Medium depth range - about 1/5 of the maximum used C1C2 distance. Medium side coverage.

Resolution
Medium resolution - sufficient rather for detailed investigation of shallow structures.

Measuring conditions
Commonly used array for various ground resistivity. Medium resistance against electric noise is caused by lower level of measured potentials.

Wenner

Purpose
The fastest array. The most frequent variant called Wenner alpha is close to Schlumberger with similar range of applications. Other variants called Wenner beta (close to Dipole-Dipole) and Wenner gamma (non conventional array) are used rarely.

Section coverage
Low depth range – about 1/6 of the maximum used C1C2 distance. Low side coverage.

Resolution
Low resolution – inconvenient for detailed investigation of deeper structures.

Measuring conditions
High resistance against electric noise – effective replacement of Schlumberger at places hit by electric noise.

Dipole-Dipole

Purpose
The most detailed array especially for detection of vertical structures (including slimmer fissures, ore veins) and cavities.

Section coverage
Medium depth range – about 1/5 of the maximum used C1C2 distance. Medium side coverage.

Resolution
The highest resolution – allows the maximum possible distinguishing of deeper situated structures.

Measuring conditions
The effective depth range is significantly limited by rapid decrease of measured potential at larger dipole distance. Artificial electric noise causes another important limitation of use of this array.

Pole-Dipole

Purpose
The most effective array for detection of all vertical structures (even slim crackles) with high depth range.

Section coverage
High depth range – about 1/3 of the used length of the electrode array. Higher side coverage.

Resolution
Higher resolution. The accuracy of positions in section is decreased (side shift) as the array is non symmetric. For better results (regarding positions) it is recommended to use an additional Reverse Pole-Dipole or to use Combined Pole-Dipole instead.

Measuring conditions
Installation of external current electrode C2 (C1 in the case of reverse array) – called infinite – is necessary. The distance of the infinite electrode should be at least five times bigger than the maximum length of used electrode array. Its optimum position should be in perpendicular direction from the electrode array. The big distance of infinite current electrode requires maximum power of the transmitter and careful installation of such an electrode (or even electrode nest) to provide its lowest possible ground resistance.

Pole-Pole

Purpose

The most effective array for investigation of deep structures (all kinds). Rarely used.

Section coverage

The highest depth range - almost 70 % of the length of the electrode array. The highest side coverage.

Resolution

Low resolution.

Measuring conditions

Installation of two external electrodes (C2 and P2) – called infinites – is necessary. The preparation of the measurement is the most time consuming with the highest requirement regarding the available free area around the measured line. Each infinite electrode should be at least at the distance of 5 multiple of the maximum length of used electrode array. Their optimum position should be in perpendicular direction from the electrode array. C2 and P2 should be on opposite sides of the electrode array. The big distance of infinite current electrode requires maximum power of the transmitter and careful installation of such an electrode (or even electrode nest) to provide its lowest possible ground resistance.

GF Instruments, s.r.o.
Geophysical Equipment and Services

Comparison of sections measured on the same line using different electrode arrays

This way it is possible to judge differences in section coverage (depth and side ranges) and resolution (density of measured points).

The length of the measured profile: 31 m Number of electrodes: 32 (4 sections)

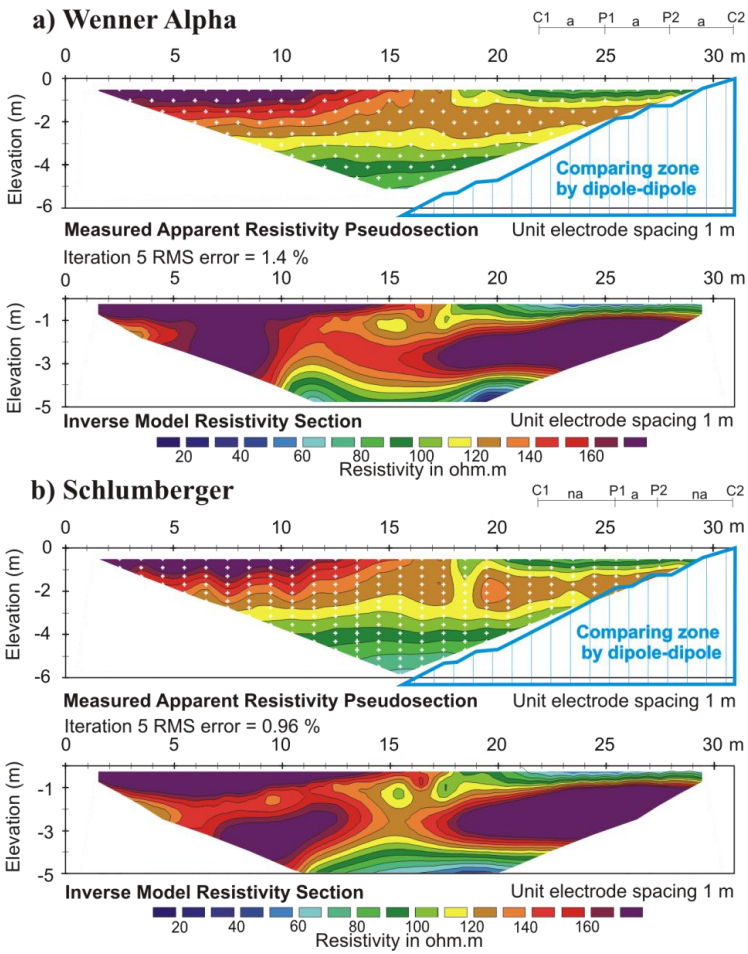

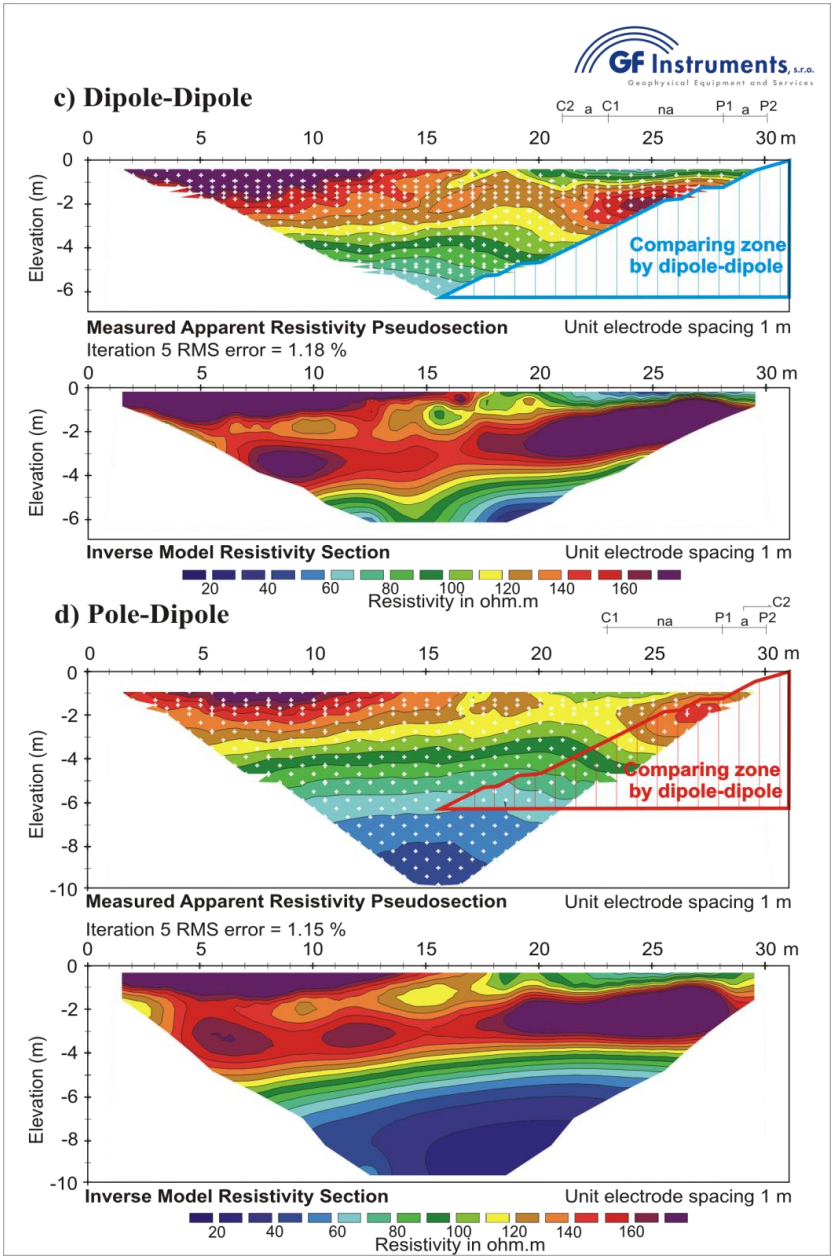
GF Instruments, s.r.o.
Geophysical Equipment and Services
c) Dipole-Dipole
C2 a C1 na P1 a P2
0 5 10 15 20 25 30 m
Elevation (m)
0 -2 -4 -6
Comparing zone by dipole-dipole
Measured Apparent Resistivity Pseudosection
Unit electrode spacing 1 m
Iteration 5 RMS error = 1.18 %
Inverse Model Resistivity Section
Unit electrode spacing 1 m
20 40 60 80 100 120 140 160
Resistivity in ohm.m
d) Pole-Dipole
C1 na P1 a P2 C2
0 5 10 15 20 25 30 m
Elevation (m)
0 -2 -4 -6 -8 -10
Comparing zone by dipole-dipole
Measured Apparent Resistivity Pseudosection
Unit electrode spacing 1 m
Iteration 5 RMS error = 1.15 %
Inverse Model Resistivity Section
Unit electrode spacing 1 m
20 40 60 80 100 120 140 160
Resistivity in ohm.m

e1) Pole-Pole

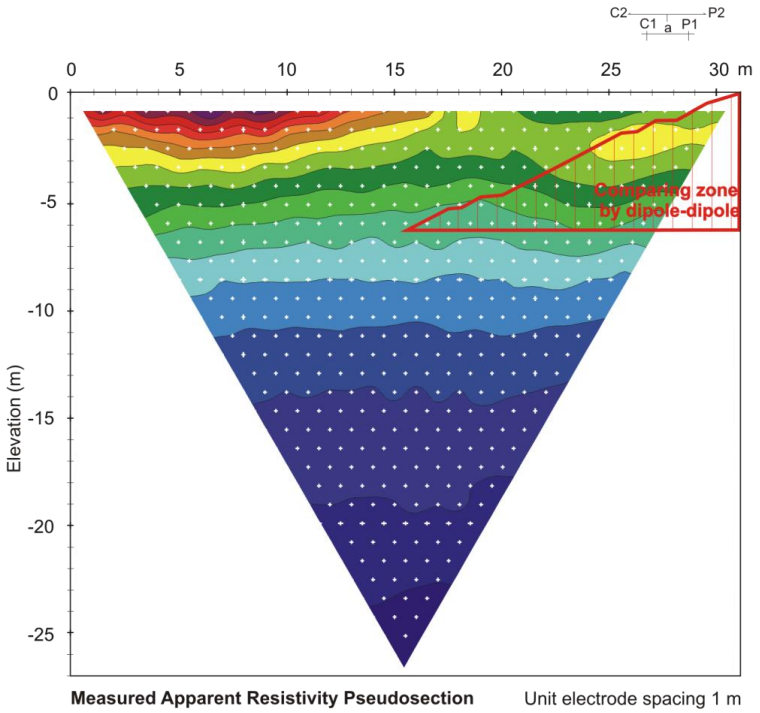

Measured Apparent Resistivity Pseudosection Unit electrode spacing 1 m

GF Instruments, s.r.o.
Geophysical Equipment and Services

e2) Pole-Pole

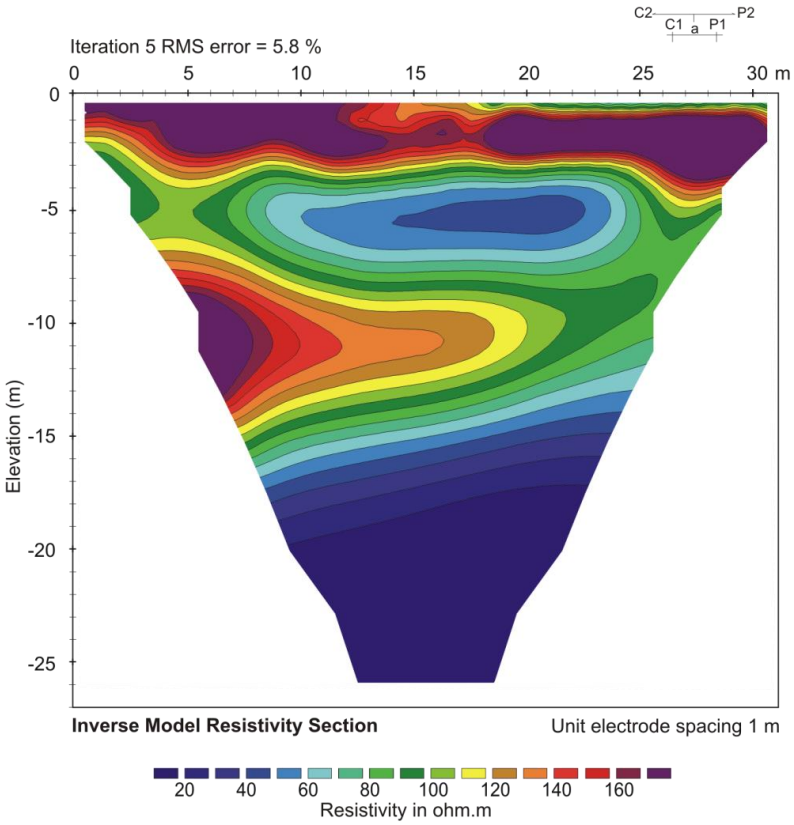

GF Instruments, s.r.o.
Geophysical Equipment and Services

Comparison of sections measured on the same line using different Wenner methods (alpha, beta, gamma)

The following pictures show different depth ranges, resolutions and sensitivities to the structure.

The length of the measured profile: 31 m Number of electrodes: 32 (4 sections)

a) Wenner Alpha

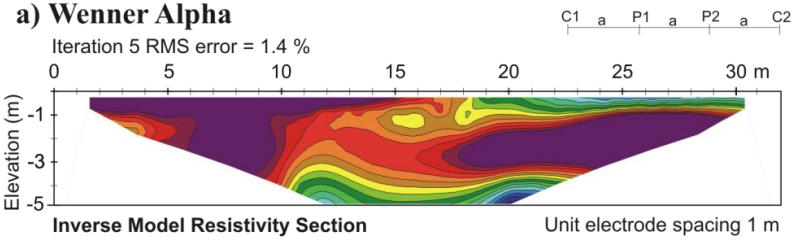

b) Wenner Beta

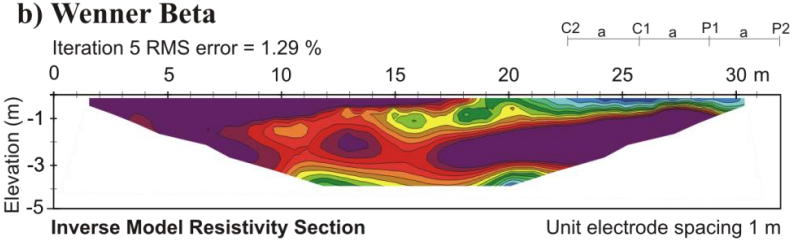

c) Wenner Gamma

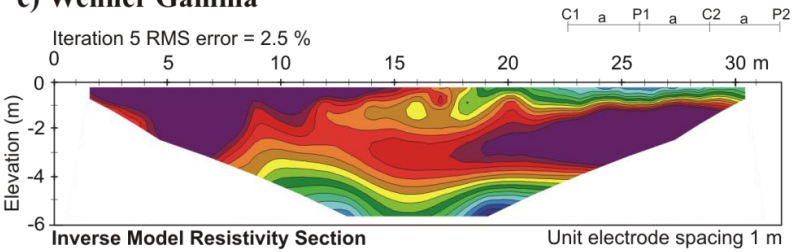

Comparison of depth-sensitivity for different electrode arrays

This picture compares sensitivity curves of different electrode arrays, when cumulative of all individual functions (75% of area under the curve) is set to be at 2 m depth. Both Schlumberger and Pole-Dipole con-figurations share the same curve for the same *a* and *n*; however Schlumberger needs greater length of the measured profile in such case.

Schlumberger and Pole-Dipole:
a = 0.6 m, n = 5
Wenner Alpha:
a = 2.3 m
Dipole-Dipole:
a = 1.4 m, n = 3
Pole-Pole:
a = 1 m

Theoretical derivation of these functions is at the end of the brochure.

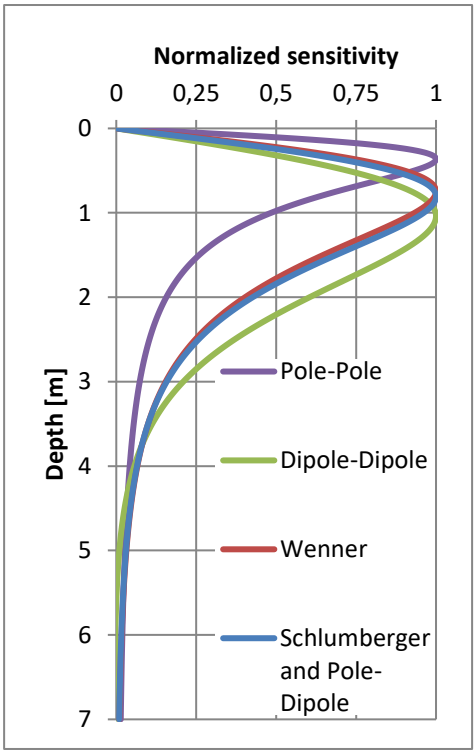

GF Instruments, s.r.o.
Geophysical Equipment and Services

Comparison of inverse model resistivity sections obtained from measurement on the artificially prepared rectangular pit (6 x 8 x 4 m) in loess filled with gravel

These pictures show different accuracy of imaging (shape, size, depth) of the pit (black line frame) and impacts on imaging of the surrounding structures.

The length of the measured profile: 47 m Number of electrodes: 48

a) Schlumberger

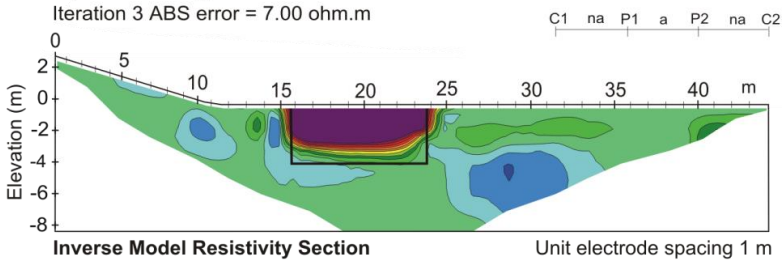

Inverse Model Resistivity Section Unit electrode spacing 1 m

b) Schlumberger Inverse

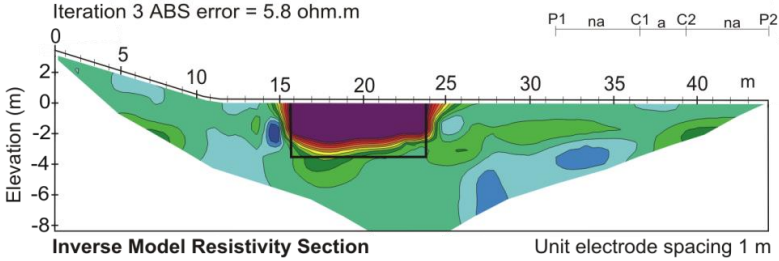

Inverse Model Resistivity Section Unit electrode spacing 1 m

c) Schlumberger HD

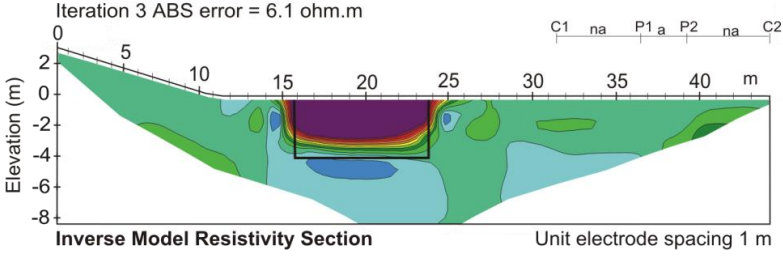

Inverse Model Resistivity Section Unit electrode spacing 1 m

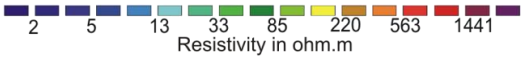

d) Dipole-Dipole

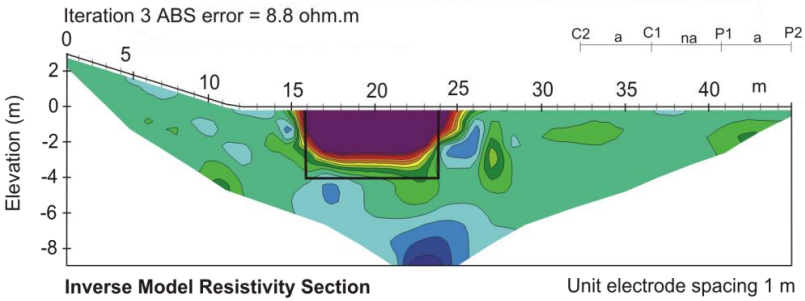

e) Dipole-Dipole HD

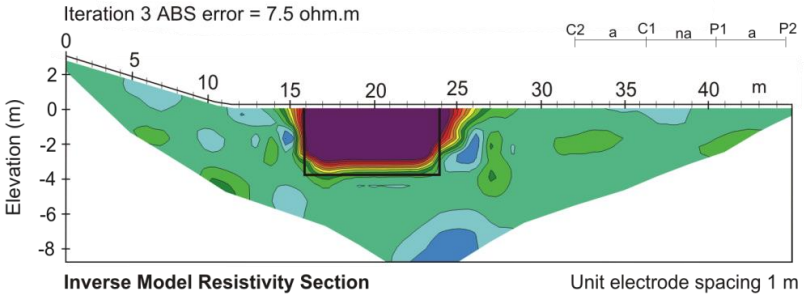

f) Pole-Dipole

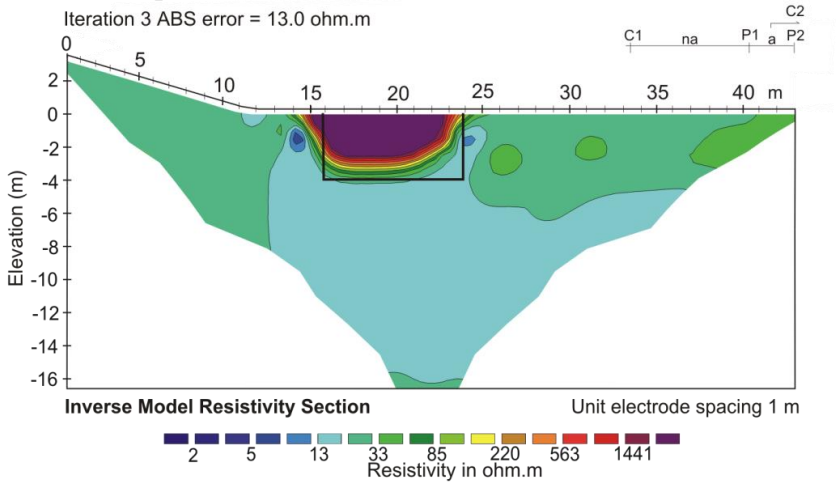

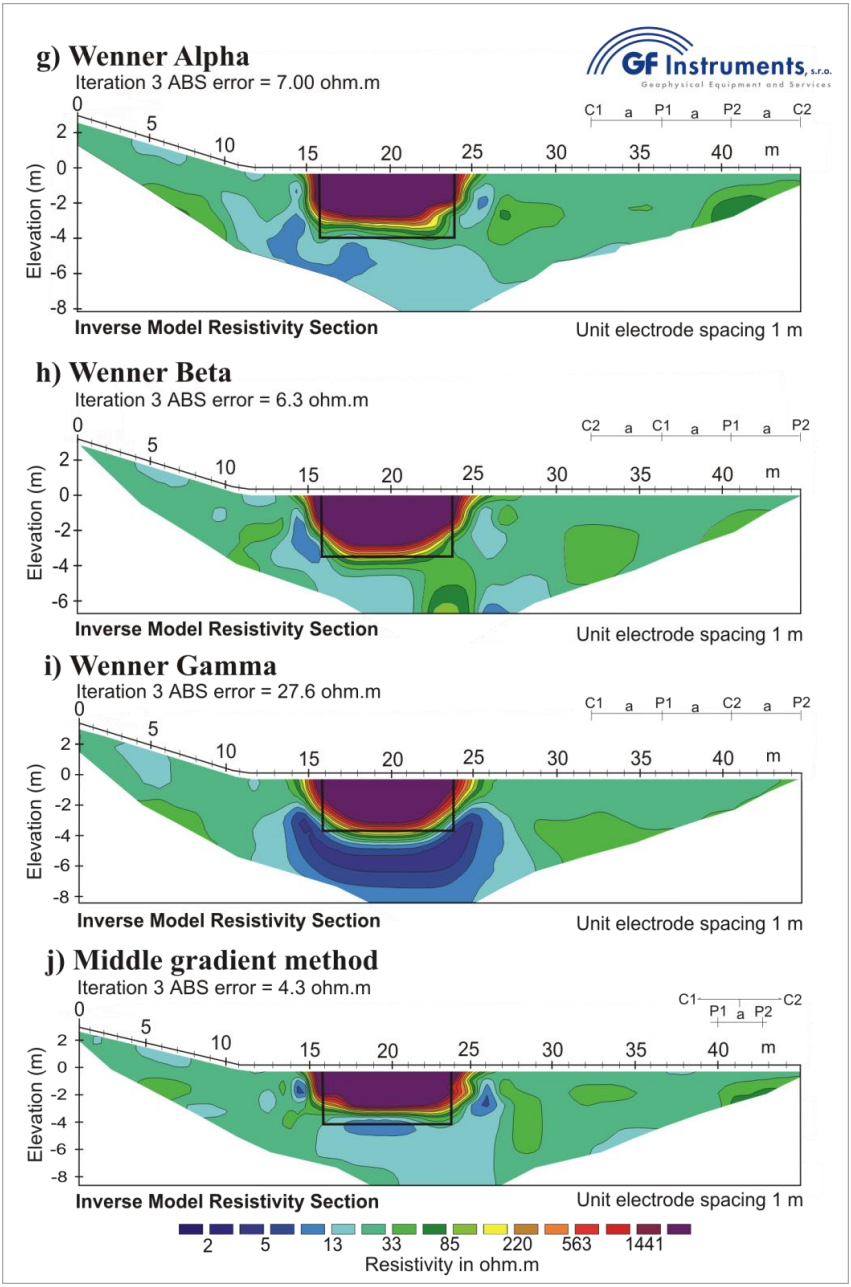
g) Wenner Alpha
Iteration 3 ABS error = 7.00 ohm.m
C1 a P1 a P2 a C2
Elevation (m)
Inverse Model Resistivity Section
Unit electrode spacing 1 m
h) Wenner Beta
Iteration 3 ABS error = 6.3 ohm.m
C2 a C1 a P1 a P2
Elevation (m)
Inverse Model Resistivity Section
Unit electrode spacing 1 m
i) Wenner Gamma
Iteration 3 ABS error = 27.6 ohm.m
C1 a P1 a C2 a P2
Elevation (m)
Inverse Model Resistivity Section
Unit electrode spacing 1 m
j) Middle gradient method
Iteration 3 ABS error = 4.3 ohm.m
C1 C2
P1 a P2
Elevation (m)
Inverse Model Resistivity Section
Unit electrode spacing 1 m
2 5 13 33 85 220 563 1441
Resistivity in ohm.m

GF Instruments, s.r.o.
Geophysical Equipment and Services

Inverse model resistivity slices and sections obtained from measurement on the artificially prepared rectangular pit (6 x 8 x 4 m) in loess filled with gravel

Measurement was performed by ARES II with active multi-electrode cable with 88 electrodes at 0.5 m spacing using Dipole-Dipole array. Electrodes were placed regularly on the rectangle circumference around the pit. Exact position of the pit is marked with black line in all slices and sections made by RES3DINV software.

Set of selected slices

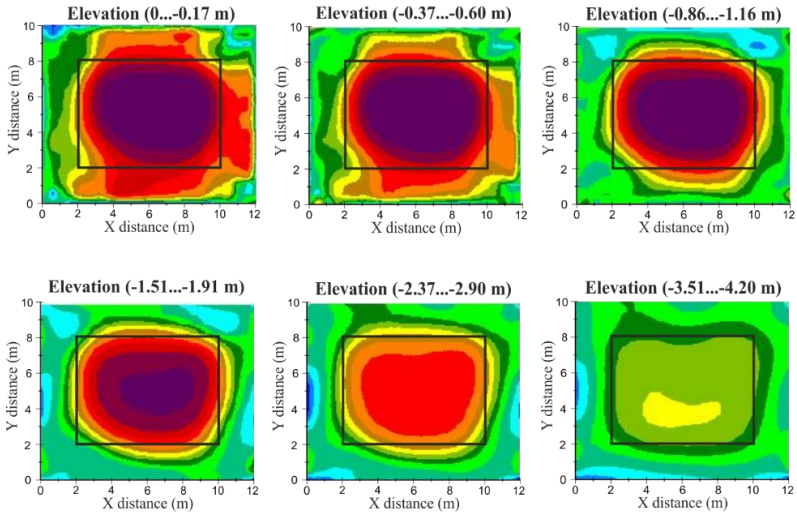

Iteration 6 RMS error = 2.93 %

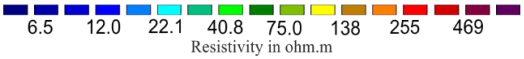

GF Instruments, s.r.o.
Geophysical Equipment and Services

Set of selected sections in X direction

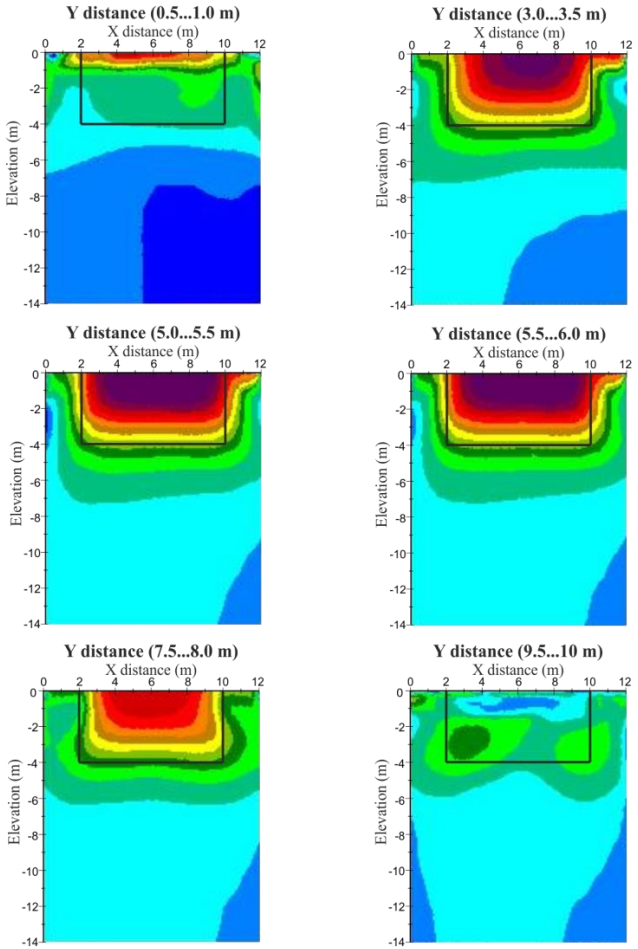

GF Instruments, s.r.o.
Geophysical Equipment and Services

Set of selected sections in Y direction

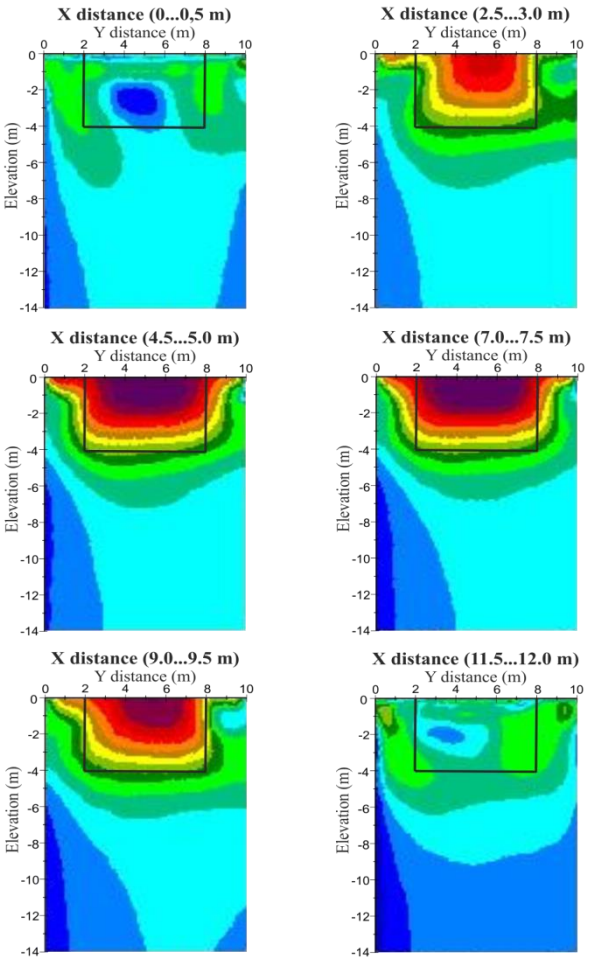

Iteration 6 RMS error = 2.93 %

Resistivity in ohm.m

Chapter 2
Examples of typical applications

Hydrogeology
This wide area of resistivity imaging applications includes various tasks:
- water management and protection
- environmental monitoring
- impacts in civil engineering

Engineering geology
This area connected with the construction and maintenance of buildings, roads, railways and bridges requires judgment of:
- bedrock surface
- slope stability
- landslide risk
- detailed geological structure
- mechanical properties of rocks, sediments etc.

Geological mapping
General survey for geological studies covers:
- raw material prospecting
- geological survey
- complex judgment of strategic localities
- choice of places for dangerous waste materials

Golden Taurus Ingeniería, S.L | Calle Tremp, 42B, 28040 Madrid
info@golden-taurus.com

GOLDEN TAURUS INGENIERÍA,S.L.

GF Instruments, s.r.o. Geophysical Equipment and Services

Projecting of water well

Detailed geological information for locating, drilling and building of water well was required. The preliminary idea of the survey was based on mapping of tectonic zones and weathered rocks. Due to the needed rather high depth range and resolution Pole-Dipole method was chosen (infinite electrode C2 at x = 50 m and y = 600 m).

The picture shows the position of a wide fault filled with permeable weathered rocks convenient for building of the well with rich water supply.

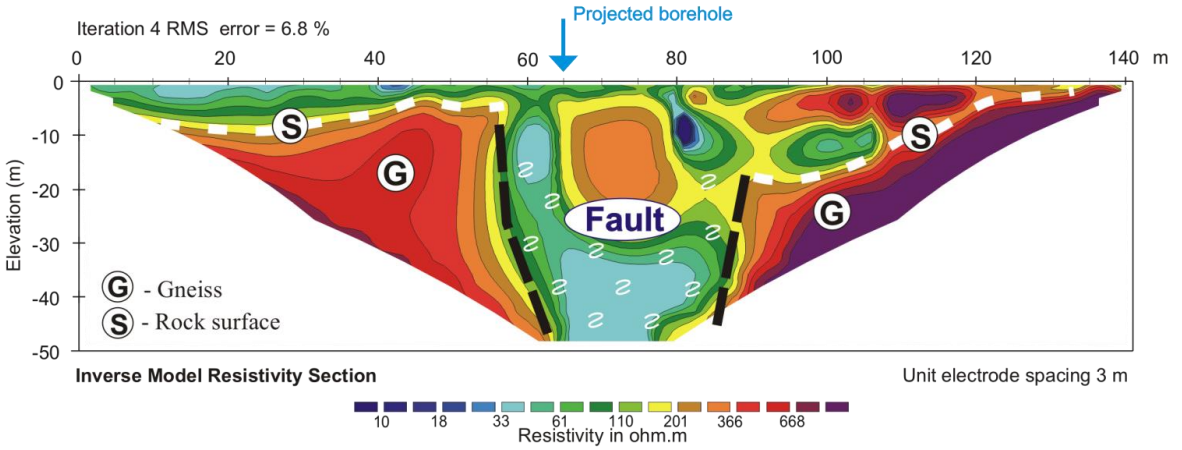

GF Instruments, s.r.o. Geophysical Equipment and Services

Golden Taurus Ingeniería, S.L | Calle Tremp, 42B, 28040 Madrid

info@golden-taurus.com

GOLDEN TAURUS INGENIERÍA,S.L.

GF Instruments, s.r.o. Geophysical Equipment and Services

Environmental protection

A complex monitoring in the frame of ground water protection in close vicinity of a pig farm was done. The goal of the resistivity imaging was to detect leakage from a liquid manure tank. Schlumberger array was used.

Under the backfill created by sand and gravel a zone with significantly decreased resistivity is seen. These extremely low values of resistivity are typical for the high contamination with organic substances.

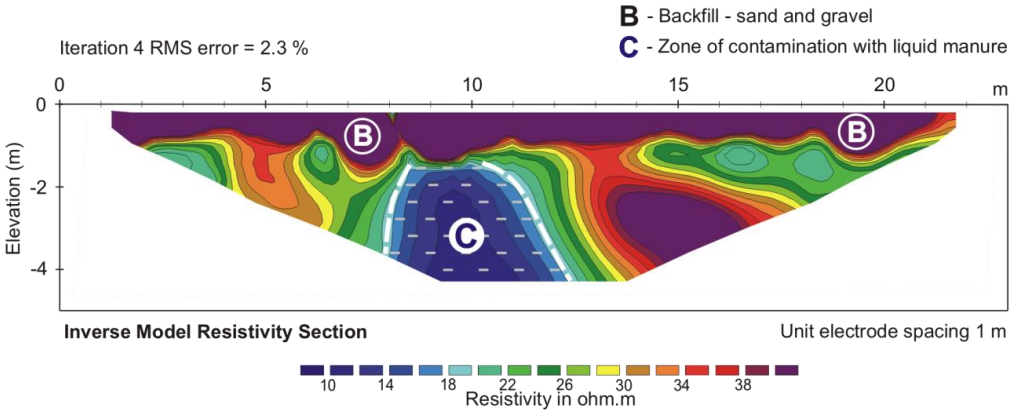

GF Instruments, s.r.o. Geophysical Equipment and Services

Protection of building

Walls of a building as well as cellars were partially hit by water coming to its insufficiently insulated basement. The survey for determination of watered zones along this building was performed. Several profiles in the vicinity of the building were measured. Schlumberger array was used.

The picture shows large watered zone with significantly decreased resisitivity in the left part. The exact position of the main water infiltration is obvious at position P.

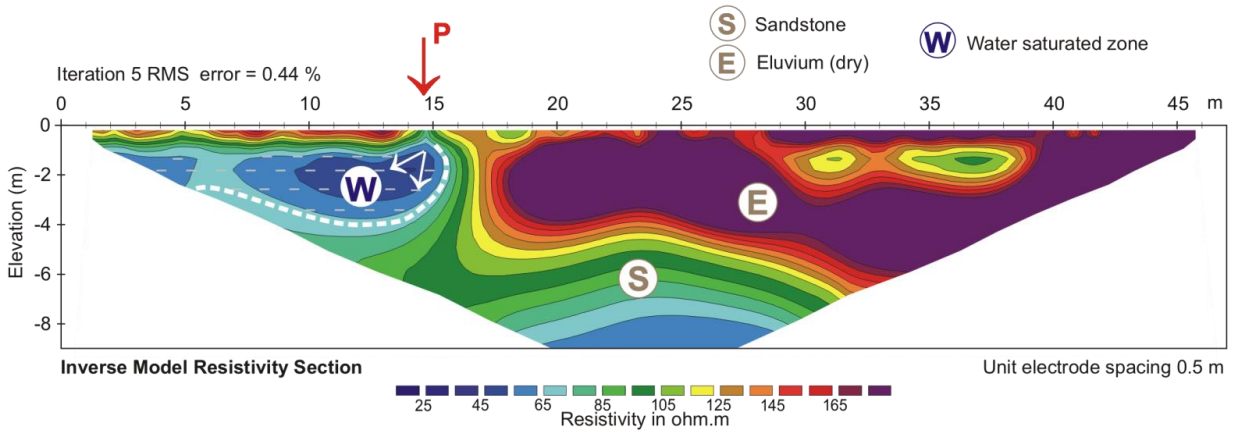

Golden Taurus Ingeniería, S.L | Calle Tremp, 42B, 28040 Madrid
info@golden-taurus.com

Golden Taurus Ingeniería, S.L | Calle Tremp, 42B, 28040 Madrid

info@golden-taurus.com

GOLDEN TAURUS INGENIERÍA,S.L.

GF Instruments, s.r.o. Geophysical Equipment and Services

River dike investigation

In the frame of the protection against floods the river dike quality and stability were monitored. Thus a profile along the dike and a dense grid of profiles perpendicularly to the river were measured. Schlumberger array was used.

The picture coming from one of profiles in perpendicular direction to the river shows both the geological structure and the base and structure of the artificial dike. The huge alluvium gravel layer allows quick water infiltration below the dike in the case of high water level. The material of the dike shows both inhomogenous structure and permeable basement which leads to its malfunction in the case of flood (quick occurrence of water on fields behind the dike).

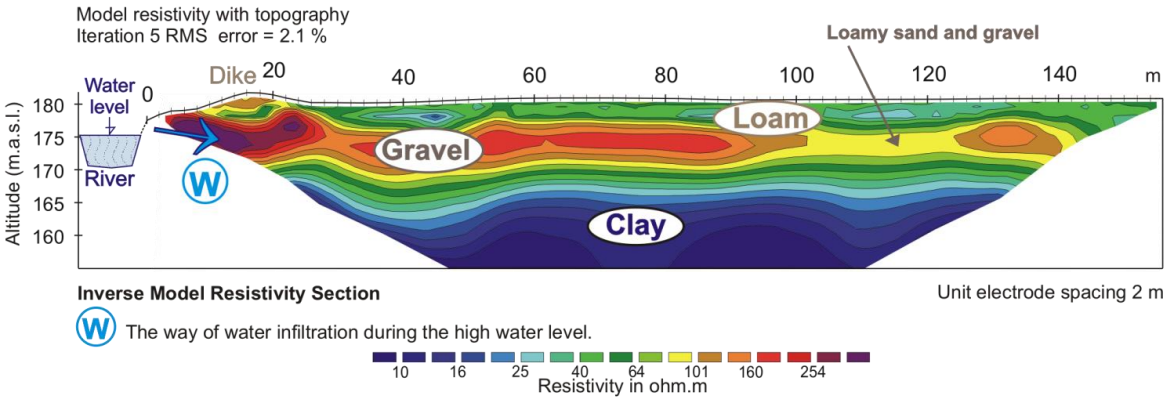

GF Instruments, s.r.o. Geophysical Equipment and Services

Golden Taurus Ingeniería, S.L | Calle Tremp, 42B, 28040 Madrid

info@golden-taurus.com

GOLDEN TAURUS INGENIERÍA,S.L.

GF Instruments, s.r.o. Geophysical Equipment and Services

Lake bottom continuous survey

Shallow lake sediments were investigated by floating multi-electrode cable (2 m spacing) and ARES II (10ch). Pole-dipole array was measured with 24 electrode cable in switching mode (upper picture). The same line was repeated using pole-dipole array with classic 10 electrode cable from 0 m to 1500 m (lower picture). Next part was done with 24 electrode cable in switching mode using simultaneous dipole-dipole and Schlumberger arrays.

Pictures show upper low resistive part with depth of 2-3 m (water and sand) followed by sandy gravel till 10 m. This layer is interrupted between 740 m and 850 m by low resistive segment (old bias river branch filled with mud). Bottom part indicates neogeny clay table.

2D imaging and inversion by Res2Dinv

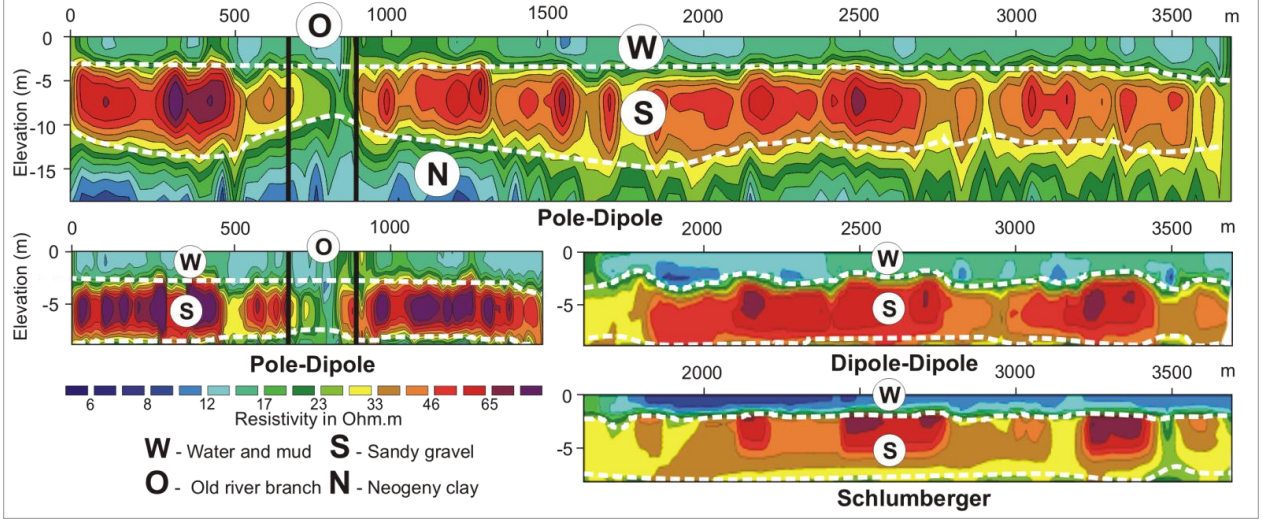

GF Instruments, s.r.o. Geophysical Equipment and Services

Golden Taurus Ingeniería, S.L | Calle Tremp, 42B, 28040 Madrid

info@golden-taurus.com

GOLDEN TAURUS INGENIERÍA,S.L.

GF Instruments, s.r.o. Geophysical Equipment and Services

Landslide risk judgement

Mapping of the depth of the debris for dam stability monitoring was done on a slope of river valley close to the dam. Schlumberger array was used.

The picture shows depth and shape of old landslide created by stones and c oarse sandstone debris. Heterogeneous structure of the bedrock partially saturated with water from the dam is obvious as well.

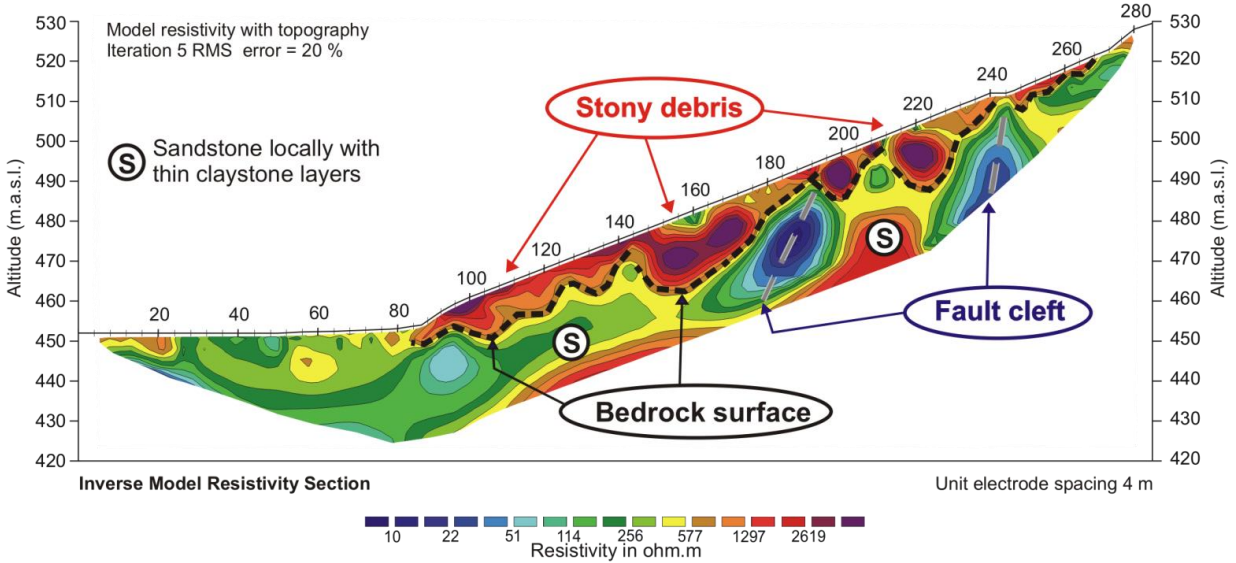

GF Instruments, s.r.o. Geophysical Equipment and Services

Golden Taurus Ingeniería, S.L | Calle Tremp, 42B, 28040 Madrid

info@golden-taurus.com

Mapping slope deformation

A road in mountains was fatally destroyed by active landslide (as a consequence of heavy rain). Detailed monitoring of the slope was performed before the road reconstruction. Schlumberger array was used.

The picture shows thickness and shape of the watered zone with risk of the massive continuous landslide. The bedrock is created by claystone and sandstone. The position of an old dry landslide is seen at position D as well.

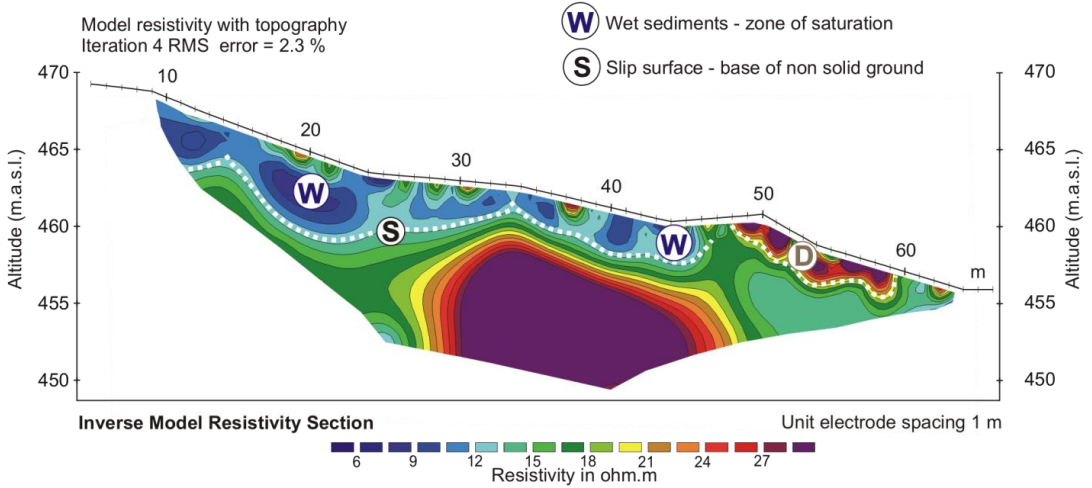

Golden Taurus Ingeniería, S.L | Calle Tremp, 42B, 28040 Madrid

info@golden-taurus.com

Monitoring slope stability above cellars

The area above a queue of wine cellars was endangered by unpredictable movement of instable soil that occurred as a consequence of collapse of some cellars. Houses and asphalt road on that place were partially destroyed. The survey should detect weak zones, holes and waste material deposits in the slope. Schlumberger array was used.

Many inhomogenities (cavities, backfill) are visible in left part of the picture. They determine the zone of the slope instability. The cellars in the right part of the picture are situated in solid rock and are not endangered by collapse.

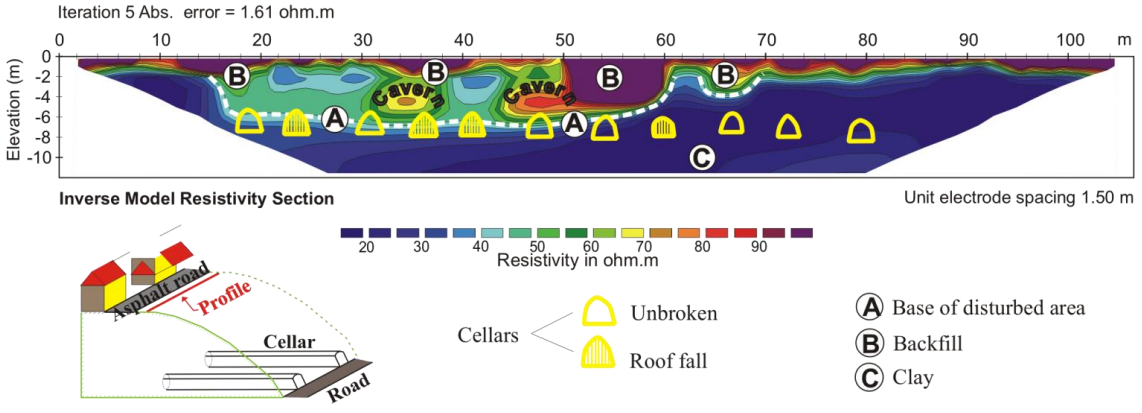

GOLDEN TAURUS INGENIERÍA,S.L.

GF Instruments, s.r.o. Geophysical Equipment and Services

Golden Taurus Ingeniería, S.L | Calle Tremp, 42B, 28040 Madrid
info@golden-taurus.com

Mapping cavities

A fishpond dam was partially destroyed during the flood. The survey was performed to detect its weak places. Schlumberger array was measured along the dam.

The section shows three main areas filled with mud from the fishpond (taken during the flood). Their positions are partially visible in situ because they are accompanied with depressions of the dam.

K1 New discovered cavity
K2 Cavity continuation
K3 Known cavity partially repaired

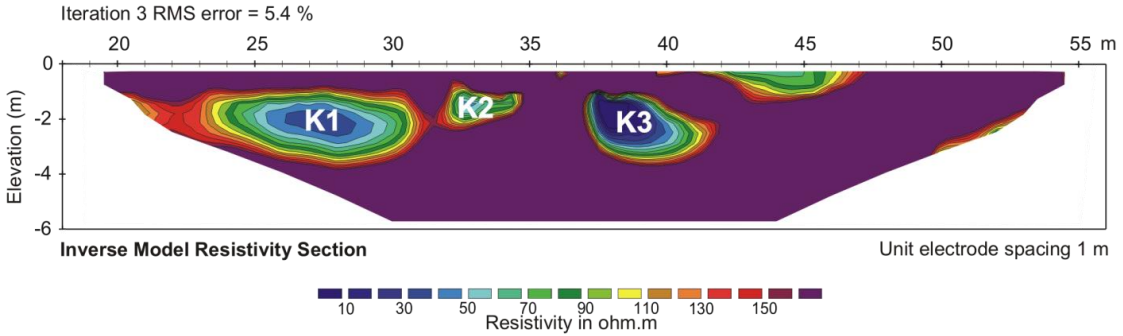

Golden Taurus Ingeniería, S.L | Calle Tremp, 42B, 28040 Madrid

info@golden-taurus.com

GOLDEN TAURUS INGENIERÍA,S.L.

GF Instruments, s.r.o. Geophysical Equipment and Services

Investigation of the rock surface

The rock surface (granodiorite) was investigated before projecting of basements of houses. Schlumberger array was used.

The shape of inclined bedrock as well as the weathered layer above are very well visible from the picture.

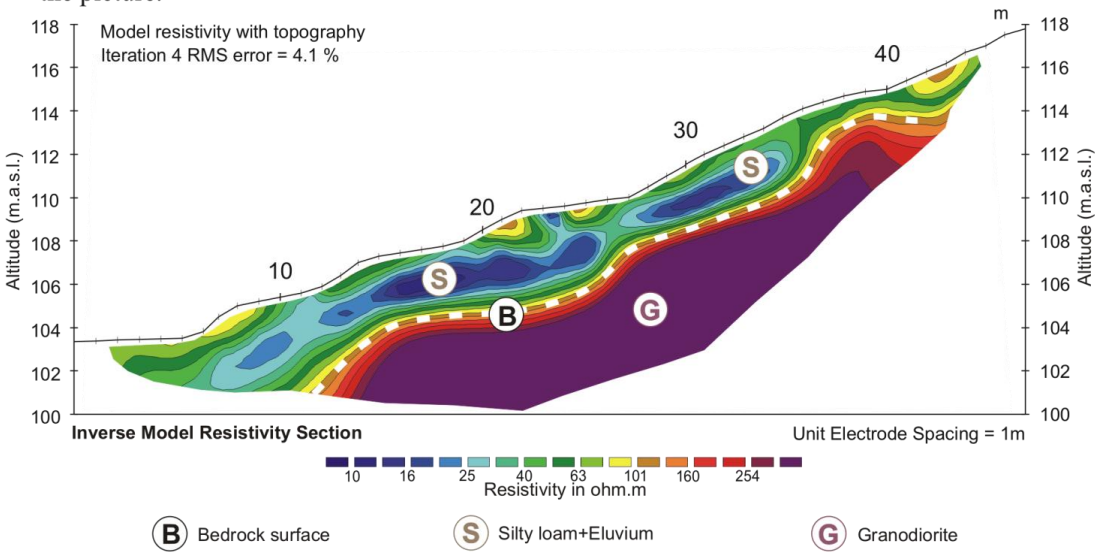

GF Instruments, s.r.o. Geophysical Equipment and Services

GF Instruments, s.r.o.
Geophysical Equipment and Services

Mapping resistivity contact

General geological mapping was performed to determine the safe area for a large building construction. The task was to give an exact information about square and depth of homogenous geological structure. Schlumberger array was used.

The picture shows the border between homogenous clay sediment and inhomogeneous area created by sandy and clayey sediments. (These two pictures demonstrate the fact that for this purpose the increased spacing - 2 m instead of 1 m - gives very similar results.)

a) Electrode spacing 2 m

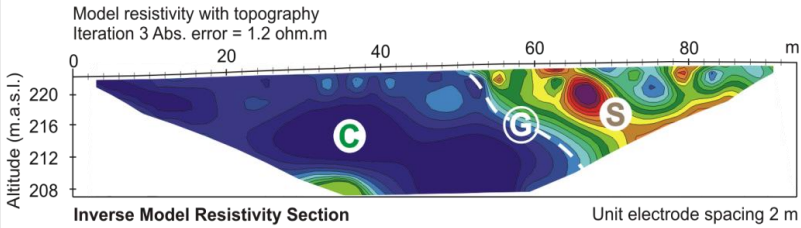

Inverse Model Resistivity Section — Unit electrode spacing 2 m

b) Electrode spacing 1 m

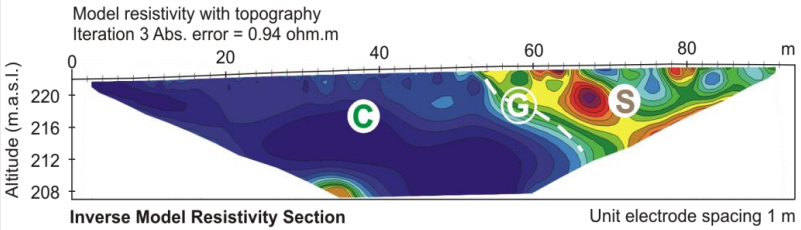

Inverse Model Resistivity Section — Unit electrode spacing 1 m

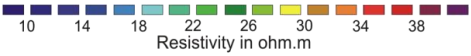

S Sandy developments C Clay sediments G Geoelectrical boundary

Golden Taurus Ingeniería, S.L | Calle Tremp, 42B, 28040 Madrid

info@golden-taurus.com

GOLDEN TAURUS INGENIERÍA,S.L.

GF Instruments, s.r.o. Geophysical Equipment and Services

Mapping backfill

The backfill thickness was determined by means of resistivity imaging. Schlumberger array was used.

It is possible to see very homogenous bedrock (clayey silt) covered by approx. 2 m backfill. The backfill shows very inhomogeneous structure (building waste material, concrete blocks and recycling material).

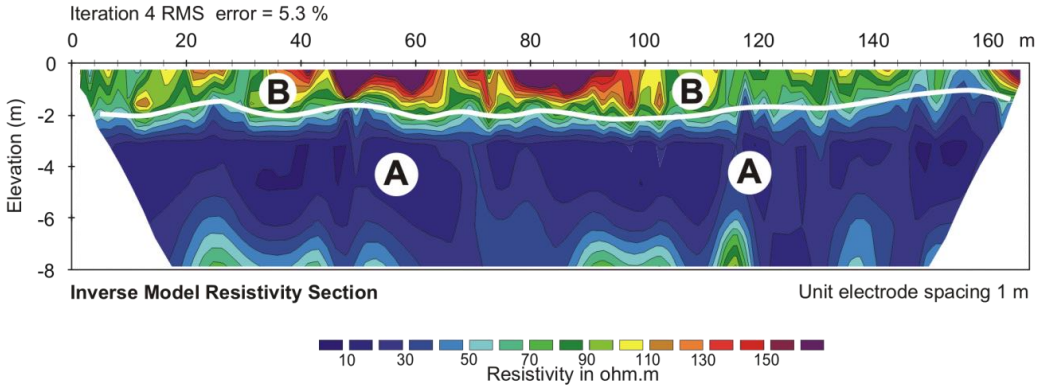

A Alluvium sediments - clayey silt

B Backfill - building garbage, concrete blocks, recycling materials

GF Instruments, s.r.o. Geophysical Equipment and Services

GF Instruments, s.r.o.
Geophysical Equipment and Services

Thin horizontal layer survey

The task was to determine a thin inhomogeneous layer (of approx. 1 m) in the ceramic clay quarry. Schlumberger array was used.

The detected inhomogeneous layer of sandstone with pyrite was spread horizontally at about 1 m depth.
(These two pictures demonstrate the necessity of the sufficient density of electrodes for required resolution.)

a) Electrode spacing 0.4 m

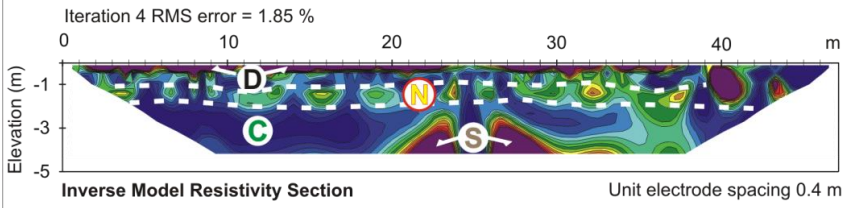

Inverse Model Resistivity Section Unit electrode spacing 0.4 m

b) Electrode spacing 0.8 m

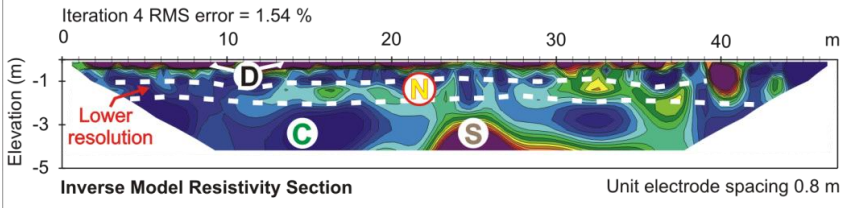

Inverse Model Resistivity Section Unit electrode spacing 0.8 m

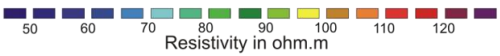

D Dry cracked claystone at the surface **S** Sandstone **C** Claystone

(N) Near-surface inhomogeneous layer- sand and insulated dissemination of metallic sulfides (pyrite)

Short guide for induced polarization tomography

Chapter 3
General features and purpose of IP measurement

Measurement of induced polarization allows distinguishing structures according to their chargeability and can be used as complementary method for resistivity tomography. Thus we can obtain useful information from simultaneous sections of resistivity, chargeability, metal factor (defined as ratio of chargeability and resistivity) and other derived quantities as slope of IP response decay curve and current-off voltage intercept. This comparison is useful for judgment of structures if raw material (e.g. metal ore, graphite, bentonite) deposit, water table level or influence of artificial substances (like oil, organic and inorganic chemicals) are investigated.
Although IP measurement is not such a general method as resistivity tomography, for some tasks can bring results that can be hardly replaced by another geophysical method. Proper application of IP usually requires deeper knowledge and consideration than resistivity measurement. Good starting idea about estimated features of studied structure always makes the methodical decision easier. ARES II system offers both traditional way of IP evaluation and advanced time effective procedures for IP measurement using up to 20 time windows with selectable width.

Physical background

To understand physical basis of IP method a comparison with simple and well known electric elements like resistor and capacitor is useful. Some structures (e.g. dry sandy rocks) look like resistor rather than capacitor – the potential induced during current pulse is rapidly lost (during milliseconds) when the pulse is terminated. Other structures (e.g. metal ore layer) look like capacitor rather than resistor – the potential induced during current pulse is kept for longer period (during seconds or longer) after the pulse is terminated. The decay curve of potential can be sampled and sections from individual sampling windows can be processed as chargeability (resp. as metal factor or other above mentioned derived quantities).

Choice of IP windows

Proper choice of IP windows can influence selectivity to specific kinds of objects with different size, depth, chemical and physical features and thus with different speed of polarization. Decay curve of induced polarization may consist of several partial exponential decay curves with different time constants due to occurrence of several objects with different features.
Following picture shows the influence of IP window selection. The section of 0.02-0.04 s window emphasizes smaller objects situated near surface. Deep objects are suppressed.
The section of 0.46-1.12 s window (Newmont 2-2-1) omits small objects near surface and emphasizes bigger and deeper situated objects.
Two remaining sections between them well illustrate the fluent change both of depth/size sensitivity and of IP scale.

GF Instruments, s.r.o.
Geophysical Equipment and Services

IP window selection

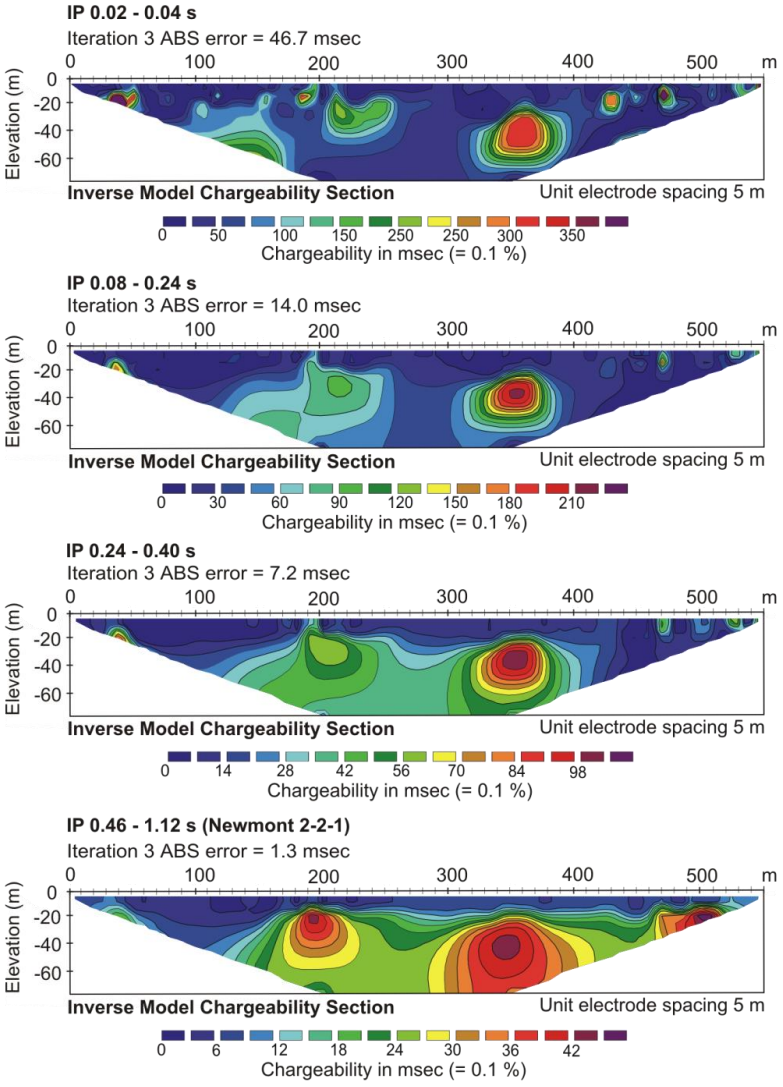

Pulse length setting

Current pulse length directly influences IP imaging in a wide range, especially if ground resistance of electrodes is high and thus low injected current requires a sufficient time for charging of structures.
Following picture shows increase of IP response and of IP imaging contrast for pulses 0.5 s, 1.0 s and 2.0 s.

It is necessary to keep ground resistances of all electrodes as low as possible (e.g. keeping ground contact watered, use of perpendicularly doubled electrodes) using the same stainless steel electrodes as for resistivity imaging (ARES II compensates voltage drift and polarization effects). The measured potential is necessary to be kept at the highest level possible to decrease noise level. It means to set 2000 mV optimum potential for IP measurement which always activates the maximum available transmitter power.

However, although the prolongation of the current pulse seems to be useful it is not commonly true that a long current pulse and classic long integral IP window yield the best IP data quality and relation with studied objects. It is useful to prove IP measurement with short (e.g. 0.5 s) pulse with series of the shortest IP windows on localities with low resistivity, especially if noise level (industrial and telluric) is high. Thus IP measurement does not prolong usual resistivity tomography and often brings additional useful information.

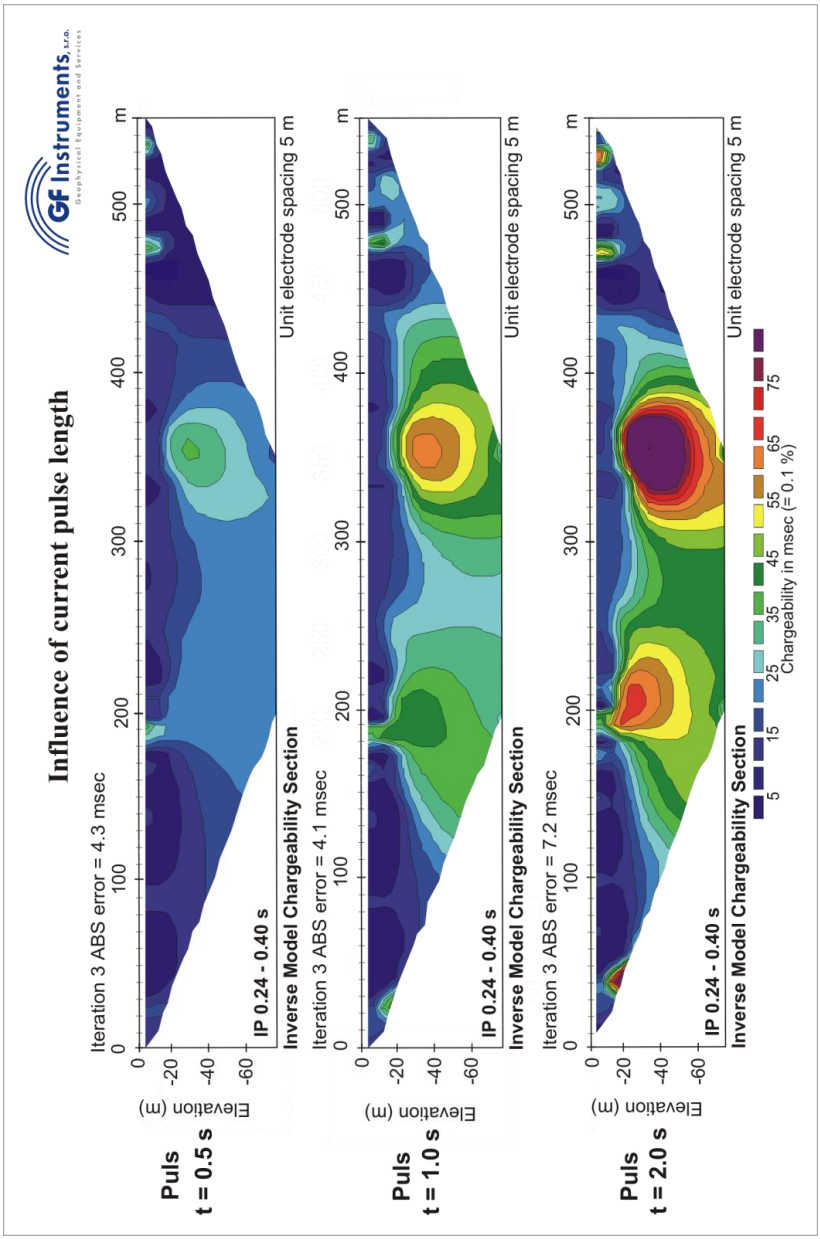
Influence of current pulse length
GF Instruments, s.r.o.
Geophysical Equipment and Services
Puls
t = 0.5 s
Iteration 3 ABS error = 4.3 msec
Elevation (m)
IP 0.24 - 0.40 s
Inverse Model Chargeability Section
Unit electrode spacing 5 m
Puls
t = 1.0 s
Iteration 3 ABS error = 4.1 msec
Elevation (m)
IP 0.24 - 0.40 s
Inverse Model Chargeability Section
Unit electrode spacing 5 m
Puls
t = 2.0 s
Iteration 3 ABS error = 7.2 msec
Elevation (m)
IP 0.24 - 0.40 s
Inverse Model Chargeability Section
Unit electrode spacing 5 m
0 100 200 300 400 500 m
0 -20 -40 -60
5 15 25 35 45 55 65 75
Chargeability in msec (= 0.1 %)

Metal factor, slope of IP response and current-off voltage intercept

These quantities are derived from measured IP and resistivity and can help with distinguishing of metal ore deposit, other IP active materials and their properties.

First two sections of the following picture show resistivity and IP in 0.24-0.40 s window. The third section showing metal factor emphasizes an ore deposit situated in low resistive vein while a bigger IP object in massive rock is suppressed.

Next picture shows two sections.
Slope of IP response decay curve distinguishes objects with different speed of discharge (negative line slope of the decay curve with logarithmic time scale).
Current-off voltage intercept shows calculated chargeability value of all IP objects immediately after the current pulse end.

These complex IP analyses together with ARES II full decay IP registration allows detailed and sophisticated IP processing.

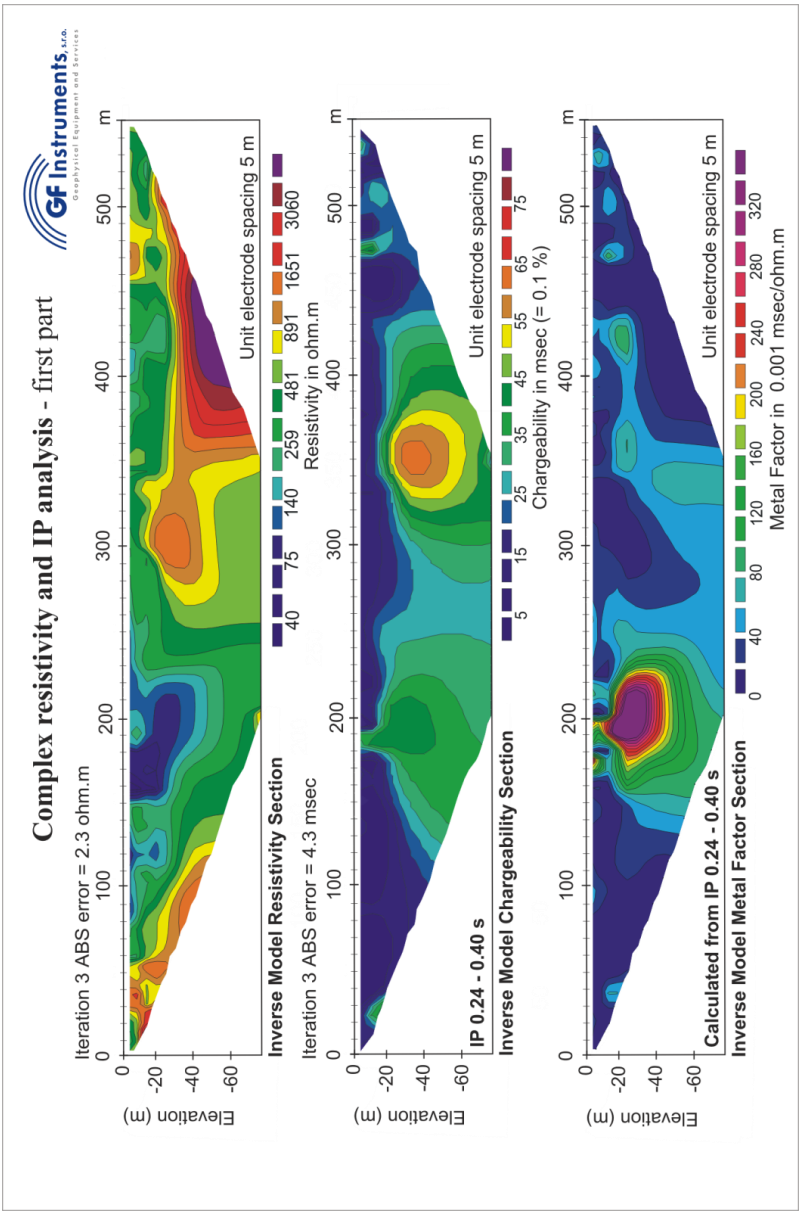
Complex resistivity and IP analysis - first part
GF Instruments, s.r.o.
Geophysical Equipment and Services
Iteration 3 ABS error = 2.3 ohm.m
Inverse Model Resistivity Section
Unit electrode spacing 5 m
40 75 140 259 481 891 1651 3060
Resistivity in ohm.m
Iteration 3 ABS error = 4.3 msec
IP 0.24 - 0.40 s
Inverse Model Chargeability Section
Unit electrode spacing 5 m
5 15 25 35 45 55 65 75
Chargeability in msec (= 0.1 %)
Calculated from IP 0.24 - 0.40 s
Inverse Model Metal Factor Section
Unit electrode spacing 5 m
0 40 80 120 160 200 240 280 320
Metal Factor in 0.001 msec/ohm.m
Elevation (m)
0 -20 -40 -60
0 100 200 300 400 500 m

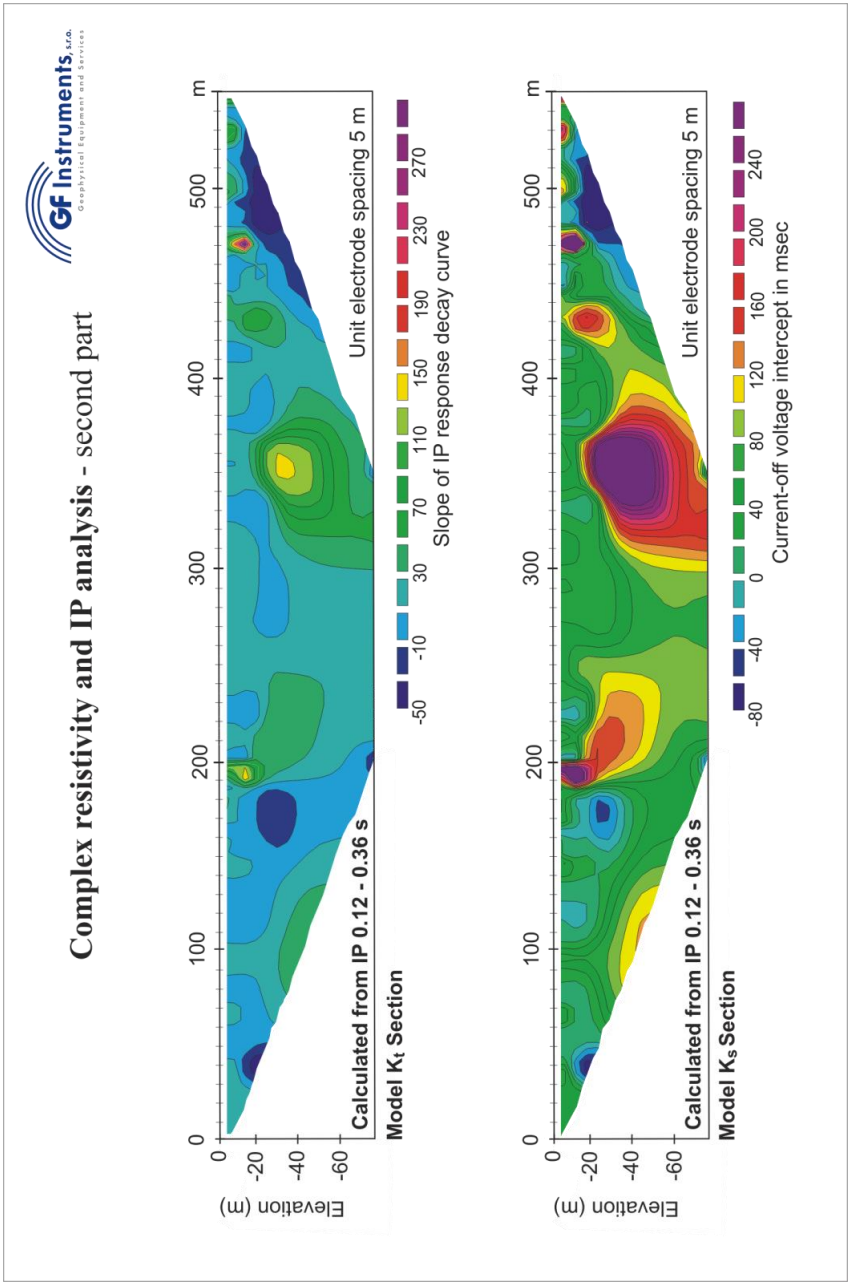
Complex resistivity and IP analysis - second part
GF Instruments, s.r.o.
Geophysical Equipment and Services
Elevation (m)
0
-20
-40
-60
0
100
200
300
400
500
m
Calculated from IP 0.12 - 0.36 s
Model K_t Section
Unit electrode spacing 5 m
-50
-10
30
70
110
150
190
230
270
Slope of IP response decay curve
Elevation (m)
0
-20
-40
-60
0
100
200
300
400
500
m
Calculated from IP 0.12 - 0.36 s
Model K_s Section
Unit electrode spacing 5 m
-80
-40
0
40
80
120
160
200
240
Current-off voltage intercept in msec

Data acquisition notes

IP measurement is often typical with significant influence of noise of industrial and telluric origin. It usually makes deep and sensitive IP measurement difficult.
Pictures on following pages illustrate differences of results obtained on a place with industrial noise using various procedures. The resistivity section shows upper loam layer, massive loess layer and eluvial part of bedrock.
IP section with stacking 4/6 (usual resistivity mode) quickly loses IP data quality with increasing depth. Random bull eyes in apparent section result in completely false and random objects in model IP section.
Consequent IP sections with stacking 6/30 and 12/60 improve stability of apparent IP sections giving smooth model IP sections after inversion. Thus IP differences less than 1% can be seen near bottom border of loam. Of course, the cost for such an improvement is significant prolongation of measuring time.
The last IP section with GF vector correction (special IP procedure) at stacking 4/6 shows at least the same data quality as the previous stacking 12/60 but the time of measurement is only two times longer than normal resistivity survey with the same stacking.

Golden Taurus Ingeniería, S.L | Calle Tremp, 42B, 28040 Madrid

info@golden-taurus.com

GOLDEN TAURUS INGENIERÍA,S.L.

GF Instruments, s.r.o. Geophysical Equipment and Services

GF Testing Site
Reference Resistivity Section

Measured with ARES II using Schlumberger array
2D imaging and inversion by Res2Dinv

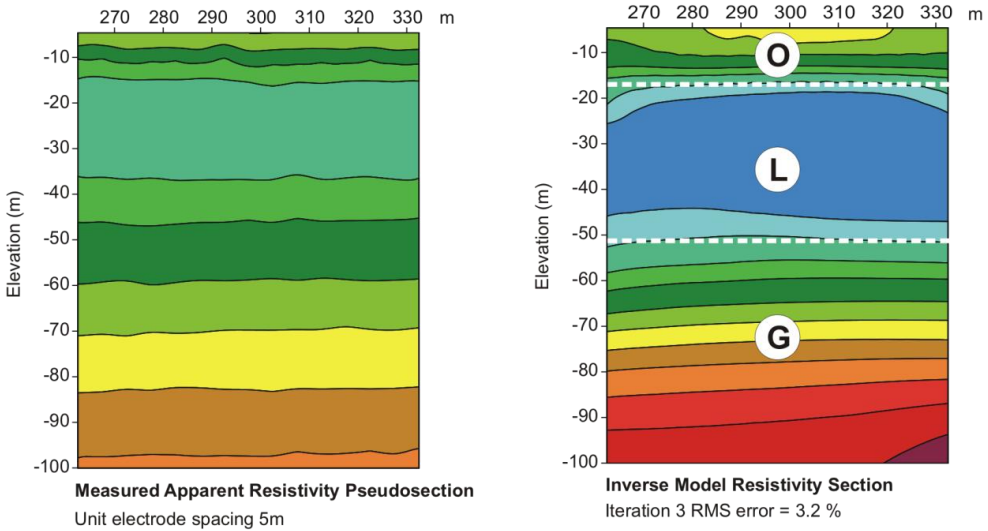

Measured Apparent Resistivity Pseudosection
Unit electrode spacing 5m

Inverse Model Resistivity Section
Iteration 3 RMS error = 3.2 %

O Overlaying clay loam **L** Loess **G** Gradual transition to a bedrock

GF Instruments, s.r.o. Geophysical Equipment and Services

Golden Taurus Ingeniería, S.L | Calle Tremp, 42B, 28040 Madrid

info@golden-taurus.com

GOLDEN TAURUS INGENIERÍA,S.L.

GF Instruments, s.r.o. Geophysical Equipment and Services

GF Testing Site
Induced Polarization Section - Stacking 4/6

Measured with ARES II using Schlumberger array
2D imaging and inversion by Res2Dinv
IP window = 0.005 - 0.025 s

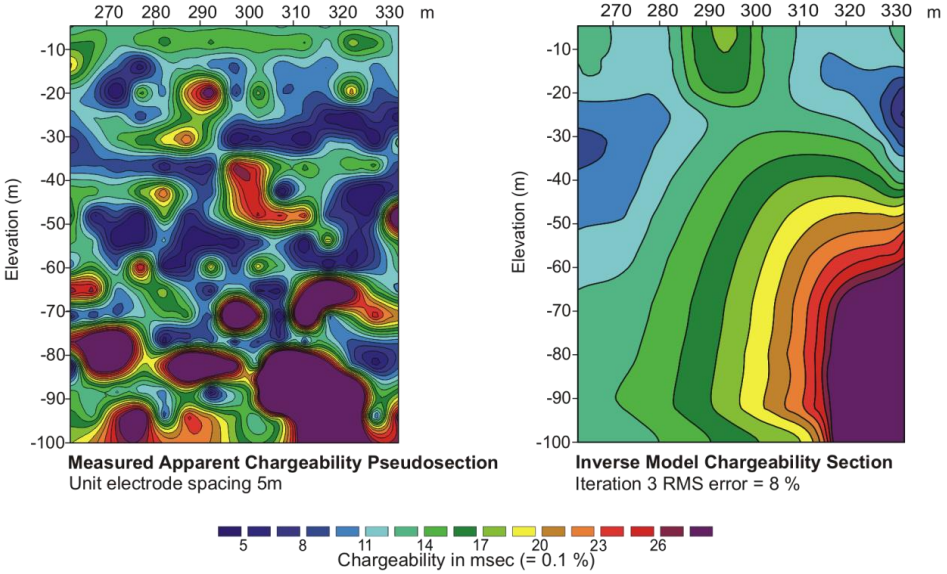

GF Instruments, s.r.o. Geophysical Equipment and Services

Golden Taurus Ingeniería, S.L | Calle Tremp, 42B, 28040 Madrid

info@golden-taurus.com

GOLDEN TAURUS INGENIERÍA,S.L.

GF Instruments, s.r.o. Geophysical Equipment and Services

GF Testing Site
Induced Polarization Section - Stacking 6/30

Measured with ARES II using Schlumberger array
2D imaging and inversion by Res2Dinv
IP window = 0.005 - 0.025 s

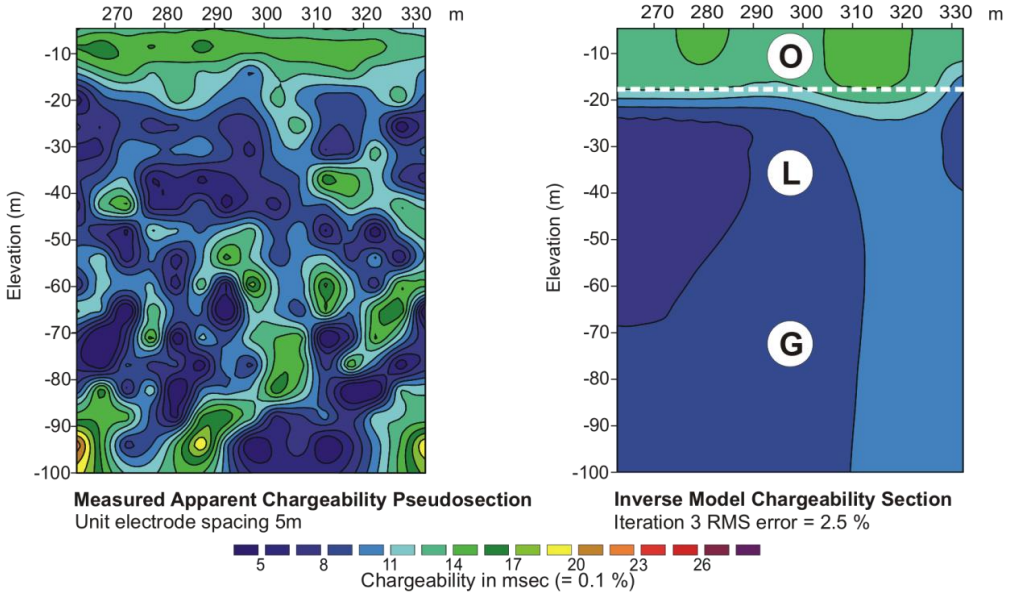

Measured Apparent Chargeability Pseudosection
Unit electrode spacing 5m

Inverse Model Chargeability Section
Iteration 3 RMS error = 2.5 %

5 8 11 14 17 20 23 26
Chargeability in msec (= 0.1 %)

O Overlaying clay loam

L Loess

G Gradual transition to a bedrock

GF Instruments, s.r.o. Geophysical Equipment and Services

Golden Taurus Ingeniería, S.L | Calle Tremp, 42B, 28040 Madrid

info@golden-taurus.com

GF Testing Site
Induced Polarization Section - Stacking 12/60

GF Instruments, s.r.o.
Geophysical Equipment and Services

Measured with ARES II using Schlumberger array
2D imaging and inversion by Res2Dinv
IP window = 0.005 - 0.025 s

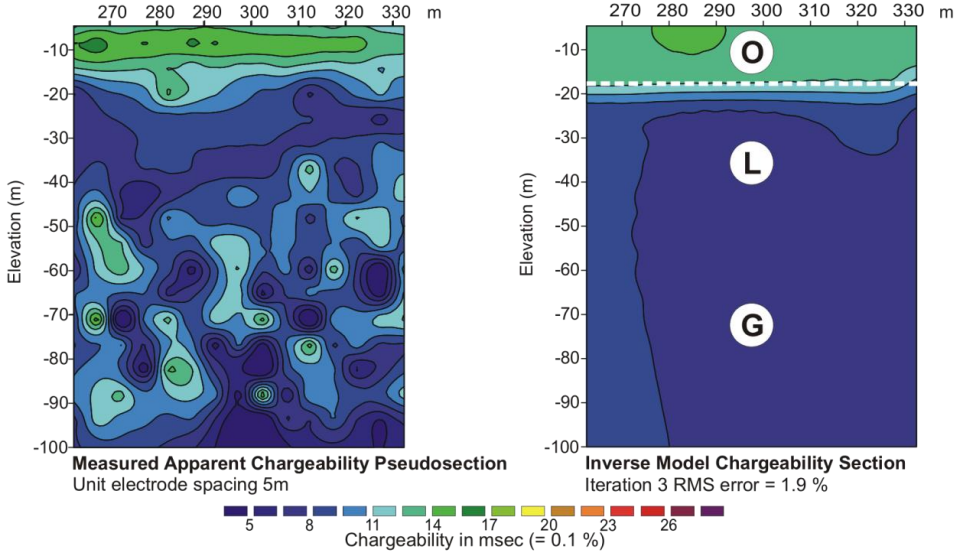

O Overlaying clay loam **L** Loess **G** Gradual transition to a bedrock

GF Instruments, s.r.o.
Geophysical Equipment and Services

Golden Taurus Ingeniería, S.L | Calle Tremp, 42B, 28040 Madrid

info@golden-taurus.com

GOLDEN TAURUS INGENIERÍA,S.L.

GF Instruments, s.r.o. Geophysical Equipment and Services

GF Testing Site

Induced Polarization Section - Vector Correction of Stacking 4/6

Measured with ARES II using Schlumberger array
2D imaging and inversion by Res2Dinv
IP window = 0.005 - 0.025 s

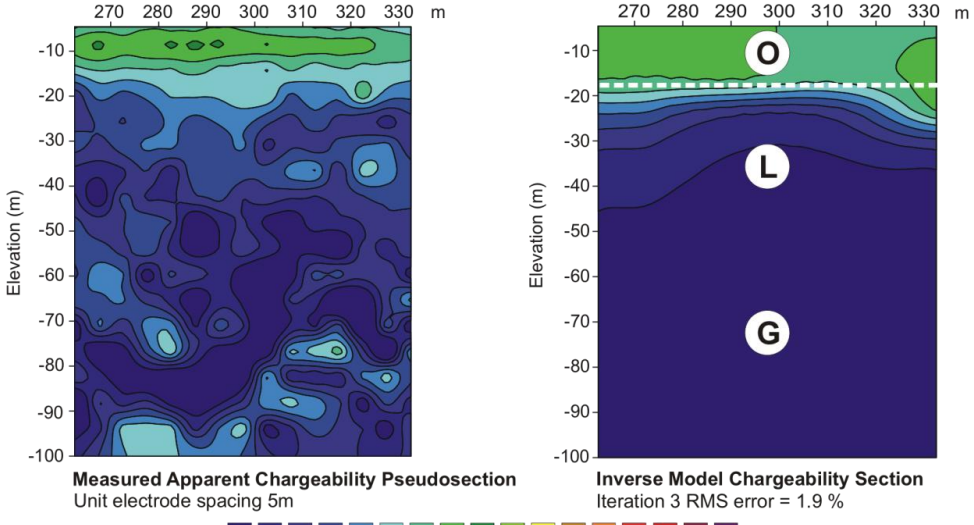

GF Instruments, s.r.o. Geophysical Equipment and Services

Chapter 4
Examples of typical IP applications

Following examples show results from **raw material prospecting** and **hydrogeology,** which belong to basic areas of IP applications.
Environmental studies like leakage of oil and other mineral substances can be supported by IP measurement as well.

Some important features of IP measurement are mentioned in individual pictures.

Ore Prospecting

Shallow situated ore deposit (former surface mines from 15th century) was investigated using Schlumberger array.
Chargeability section shows ore vein situated in weakened zone of rock characterized by lower resistivity (see resistivity section). Metal factor section illustrates further possibility of selection of ore vein positions decreasing influence of changing resistivity.

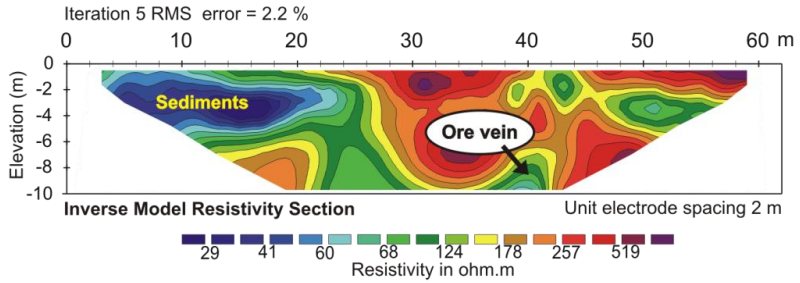

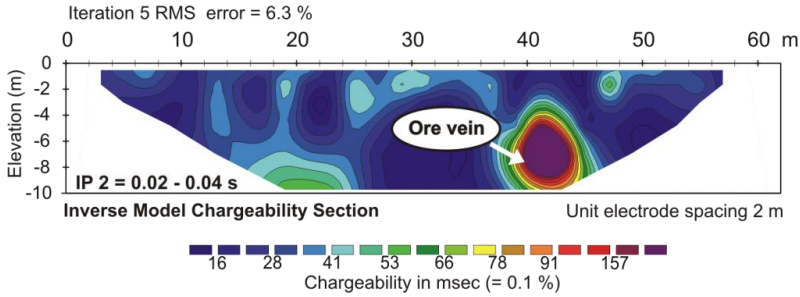

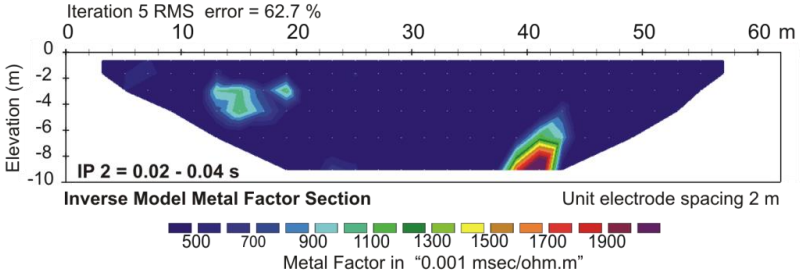

GF Instruments, s.r.o.
Geophysical Equipment and Services

IP Windows Selection

This picture (accompanying the previous one) shows the crucial influence of IP windows position in pulse decay curve. Smaller and shallow situated objects are emphasized in first 20 ms IP window while next IP windows select weakened zone filled with ore vein.

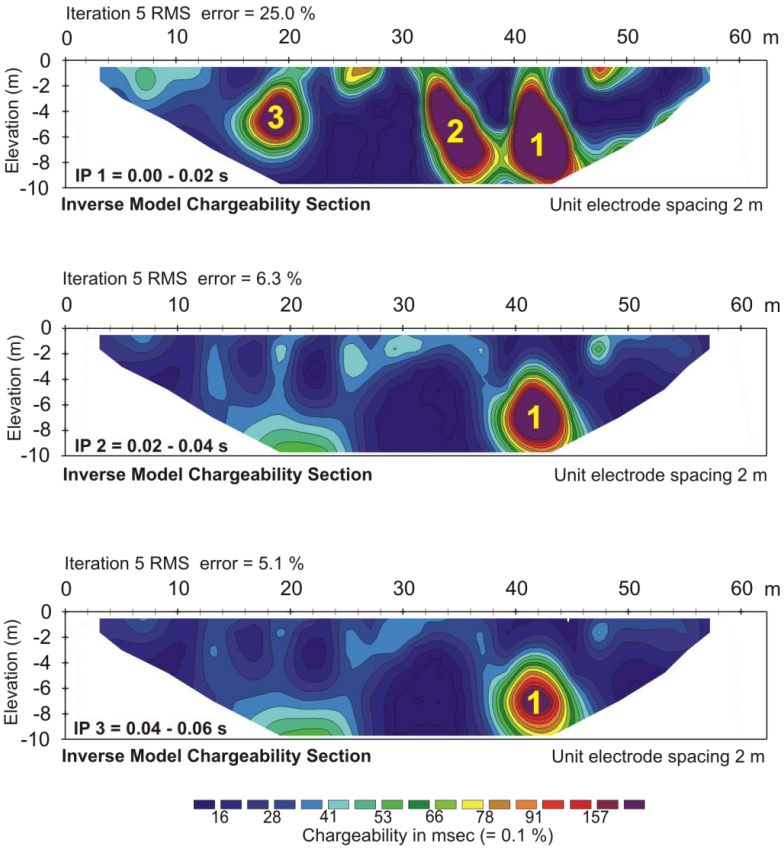

Golden Taurus Ingeniería, S.L | Calle Tremp, 42B, 28040 Madrid

info@golden-taurus.com

Natural Graphite Deposit

GF Instruments, s.r.o. Geophysical Equipment and Services

IP Section performed above former drift of graphite mine shows position of deposit. Position of the drift as well as rather complicated geological structure are seen from accompanying resistivity section.

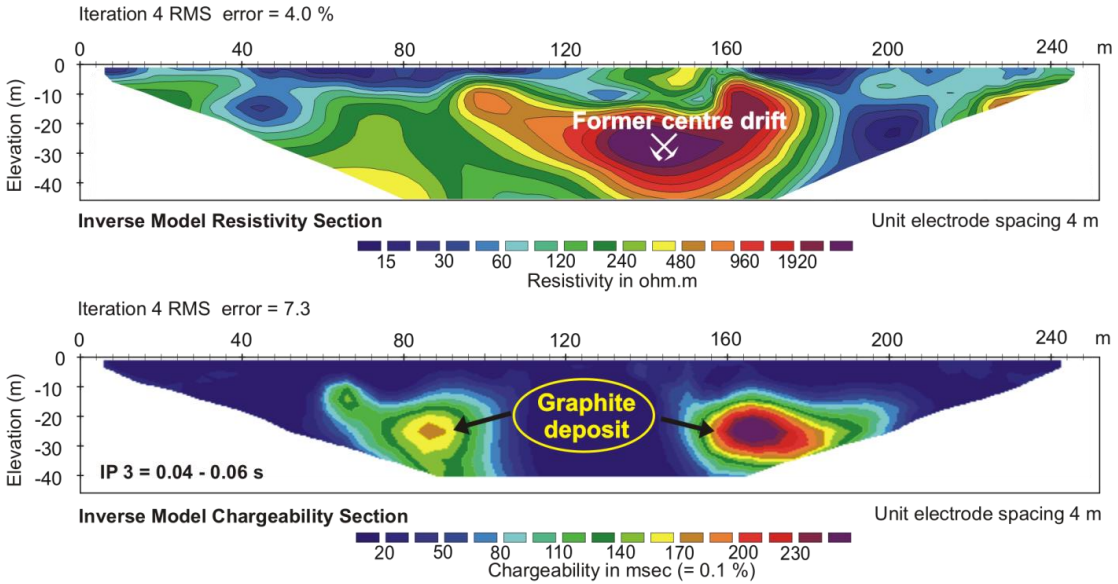

GOLDEN TAURUS INGENIERÍA,S.L.

GF Instruments, s.r.o. Geophysical Equipment and Services

GF Instruments, s.r.o.
Geophysical Equipment and Services

Water Table Investigation

Basic geology of the site is created by quartz sand above clay background visible in resistivity section.
IP section shows slightly inclined water table at approximately 3 m level in the sandy layer.

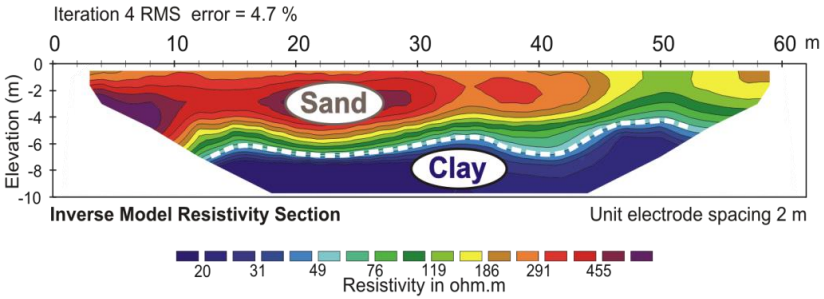

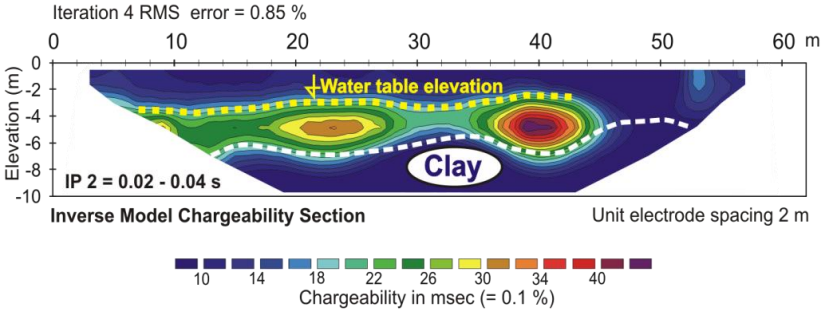

Golden Taurus Ingeniería, S.L | Calle Tremp, 42B, 28040 Madrid
info@golden-taurus.com

GOLDEN TAURUS INGENIERÍA,S.L.

GF Instruments, s.r.o. Geophysical Equipment and Services

Investigation of pegmatite deposit

Hard formation with its weathered part is seen in the resistivity section.
IP section differentiates the pegmatite vein (higher IP values) from surrounding basic rock.

Measured with ARES II using Schlumberger array, 2D imaging and inversion by Res2Dinv

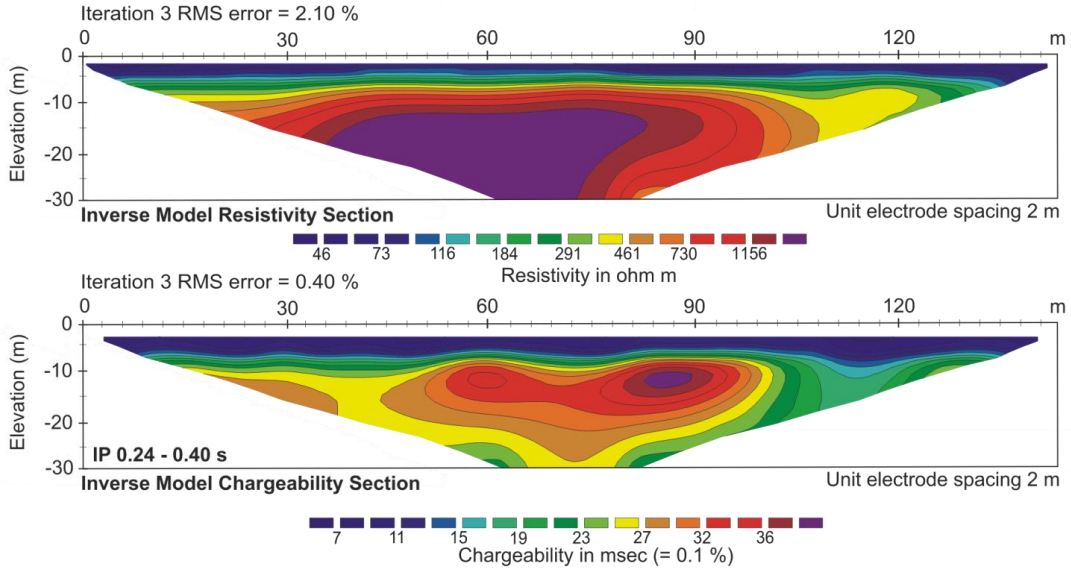

GF Instruments, s.r.o. Geophysical Equipment and Services

Theory of Depth-Sensitivity for Geoelectric Resistivity Measurement

by Hana Růžičková

This chapter brings a complete derivation with all important mathematical crossings together with physical simplifications. Thus individual sensitivity formulae for Schlumberger, Wenner, Dipole-Dipole, Pole-Dipole and Pole-Pole arrays are obtained. The approach to the definition of the sensitivity function is taken from notes by M. H. Loke published with his Res2Dinv/Res3Dinv software.

To obtain the sensitivity function we assume homogeneous earth and determine how much a change in the resistivity of a layer will influence the potential measured by the electrode. We will start with the simplest configuration: one current electrode and one potential electrode. We put the current electrode at position $\vec{c} = (c, 0, 0)$ and the potential one at $\vec{p} = (p, 0, 0)$. For electric potential defined by $\vec{E} = -\nabla\varphi$ we can write Ohm's law as

$$\vec{j} = \sigma\vec{E} = -\sigma\nabla\varphi,$$

where $\vec{E}$ is electric field, φ is potential, $\vec{j}$ is current density and σ is conductivity. Applying divergence on the equation and using the continuity equation $\nabla\vec{j} = -\frac{\partial\rho}{\partial t}$, we get

$$\nabla(\sigma\nabla\varphi) = \frac{\partial\rho}{\partial t},$$

where ρ is charge density and t is time. We assume our current electrode to be a point source, so $\rho(\vec{r}) = -q\delta(\vec{r} - \vec{c})$, where $\vec{r}$ contains spatial coordinates, q is charge satisfying $\frac{\partial q}{\partial t} = I$ and I is current we get from the electrode. This gives us

$$\nabla(\sigma\nabla\varphi) = -I\delta(\vec{r} - \vec{c}) \tag{1}$$

for the current electrode. We will carry out perturbation $\sigma \to \sigma + \delta\sigma$, $\varphi \to \varphi + \delta\varphi$, omit the second order terms and get:

$$\nabla(\sigma\nabla\delta\varphi) = -\nabla(\delta\sigma\nabla\varphi). \tag{2}$$

According to (1) we construct an equation for a fictitious point source of unit current at the location of the potential electrode

$$\nabla(\sigma\nabla G) = -\delta(\vec{r} - \vec{p}) \tag{3}$$

with boundary conditions

$$\frac{\partial G}{\partial \vec{n}} = 0, \tag{4}$$

where $\vec{n}$ is vector pointing outwards from the halfspace. Now we insert both our potential functions φ and G into the Green's second identity:

$$\int_{-\infty}^{\infty} [G\nabla(\sigma\nabla\delta\varphi) - \delta\varphi\nabla(\sigma\nabla G)]\,\mathrm{d}V = \oint_{\partial V} \sigma\left(\frac{\partial\delta\varphi}{\partial\vec{n}}G - \frac{\partial G}{\partial\vec{n}}\delta\varphi\right)\mathrm{d}S$$

We need to rearrange: the first term using equation (2), the second term using (3) and the fourth term using (4). Normal derivative of the third term can be rewritten as

$$\frac{\partial\delta\varphi}{\partial\vec{n}} = \nabla\delta\varphi\vec{n}.$$

$$\int_{-\infty}^{\infty} [-G\nabla(\delta\sigma\nabla\varphi)]\,\mathrm{d}V + \delta\varphi(\vec{p}) = \oint_{\partial V} \sigma\nabla\delta\varphi G\vec{n}\,\mathrm{d}S$$

Applying (1) on the last term and rearranging the equation, we get

$$\delta\varphi(\vec{p}) = \int_{-\infty}^{\infty} G\nabla(\delta\sigma\nabla\varphi)\,\mathrm{d}V - \oint_{\partial V} \delta\sigma\nabla\varphi G\vec{n}\,\mathrm{d}S$$

Applying the divergence theorem on the last term

$$\delta\varphi(\vec{p}) = -\int_{-\infty}^{\infty} \delta\sigma\nabla\varphi\nabla G\,\mathrm{d}V$$

We are interested in changes in resistivity ρ, not conductivity

$$\delta\sigma = \frac{\partial\sigma}{\partial\rho}\delta\rho = -\frac{1}{\rho^2}\delta\rho$$

We assume $\delta\rho$ to be a localized change; constant at its layer with volume $\delta\tau$, zero elsewhere. In accordance with Loke's notes, we get

$$\frac{\delta\varphi(\vec{p})}{\delta\rho} = \frac{1}{\rho^2}\int_{\delta\tau} \nabla\varphi\nabla G\,\mathrm{d}V \tag{5}$$

Now we need to determine potential from a point source. We start from (1) rearranged for homogeneous earth:

$$\nabla^2\varphi = -\rho I\delta(\vec{r} - \vec{c})$$

Delta functions satisfy

$$1 = \int_{-\infty}^{\infty} \delta(\vec{r})\,\mathrm{d}V = -\int_{-\infty}^{\infty} \frac{\nabla^2\varphi}{\rho I}\,\mathrm{d}V$$

We use the fact that potential from a point source must be spherically symmetrical. We need only half of the sphere surface of radius R for the halfspace.

$$-I\rho = \int_{-\infty}^{\infty} \nabla(\nabla\varphi)\,\mathrm{d}V = \oint_{\partial V} \nabla\varphi\,\mathrm{d}\vec{S} = \frac{\partial\varphi}{\partial R}\oint_{\partial V}\mathrm{d}S = \frac{4}{2}\pi R^2\frac{\partial\varphi}{\partial R}$$

Therefore

$$\varphi(\vec{r}) = \frac{I\rho}{2\pi|\vec{r}-\vec{c}|},\ G(\vec{r}) = \frac{\rho}{2\pi|\vec{r}-\vec{p}|}$$

Because we decided to scale the position of our electrodes at the x-axis, we insert divergences of potentials into (5) in Cartesian coordinates. Also we want our result to be the depth-sensitivity (z-coordinate as a parameter), so we will perform integrals only over $\mathrm{d}x$ and $\mathrm{d}y$.

$$\frac{\delta\varphi}{\delta\rho} = \frac{I}{4\pi^2}\int_{-\infty}^{\infty}\int_{-\infty}^{\infty} \frac{(x-c)(x-p)+y^2+z^2}{\left[(x-c)^2+y^2+z^2\right]^{\frac{3}{2}}\left[(x-p)^2+y^2+z^2\right]^{\frac{3}{2}}}\,\mathrm{d}x\,\mathrm{d}y$$

To solve this, we transform the integral into modified cylindrical coordinates: $x = r\cos\vartheta + \frac{c+p}{2}$, $y = r\sin\vartheta$, $|J| = r$. For brevity, we introduce $A = z^2 - \left(\frac{p-c}{2}\right)^2$, $B = z^2 + \left(\frac{p-c}{2}\right)^2$ and $C = (p-c)^2\cos^2\vartheta$.

$$\begin{aligned}
\frac{\delta\varphi}{\delta\rho} &= \frac{I}{4\pi^2}\int_0^{\infty}\int_0^{2\pi} \frac{\left(r^2+A\right)r}{\left[\left(r^2+B\right)^2 - r^2C\right]^{\frac{3}{2}}}\,\mathrm{d}r\,\mathrm{d}\vartheta \\
&= \frac{I}{4\pi^2}\int_0^{2\pi}\left[\frac{A\left(2B-C+2r^2\right)-2B^2-2Br^2+Cr^2}{C(4B-C)\sqrt{B^2+2Br^2-Cr^2+r^4}}\right]_0^{\infty}\mathrm{d}\vartheta \\
&= \frac{I}{4\pi^2}\int_0^{2\pi}\frac{A+B}{B(4B-C)}\,\mathrm{d}\vartheta \\
&= \frac{I}{4\pi^2}\frac{2z^2}{z^2+\left(\frac{p-c}{2}\right)^2}\int_0^{2\pi}\frac{\mathrm{d}\vartheta}{4z^2+(p-c)^2\sin^2\vartheta} \\
&= \frac{2Iz^2}{4\pi^2\left[z^2+\left(\frac{p-c}{2}\right)^2\right]}\frac{2\pi}{2z\sqrt{(c-p)^2+4z^2}} \\
&= \frac{2I}{\pi}\frac{z}{\left(4z^2+(c-p)^2\right)^{\frac{3}{2}}}
\end{aligned}$$

Depth-sensitivity for a pair of current and potential electrodes is then

$$\frac{\delta\varphi}{\delta\rho} = \frac{2I}{\pi}\frac{z}{[4z^2+a^2]^{\frac{3}{2}}},$$

where z is depth in the ground and a is distance between the electrodes. This formula is also published in Loke's notes.
For more complicated configurations we use two current electrodes C1($+I$) and C2(-I) and two potential electrodes P1 and P2. We get measured potential $\Delta\varphi$ using the superposition principle:

$$\begin{aligned}\Delta\varphi &= \Delta\varphi^{\mathrm{C1}}_{\mathrm{P1P2}} + \Delta\varphi^{\mathrm{C2}}_{\mathrm{P1P2}} = \varphi^{\mathrm{C1}}_{\mathrm{P1}} - \varphi^{\mathrm{C1}}_{\mathrm{P2}} + \varphi^{\mathrm{C2}}_{\mathrm{P1}} - \varphi^{\mathrm{C2}}_{\mathrm{P2}} \\ &= \frac{I\rho}{2\pi}\left(\frac{1}{\mathrm{C1P1}} - \frac{1}{\mathrm{C1P2}} - \frac{1}{\mathrm{C2P1}} + \frac{1}{\mathrm{C2P2}}\right),\end{aligned}$$

where C1P1 is distance between electrodes C1 and P1. For potential change and therefore depth-sensitivity function we can use the same principle.
Schlumberger array is symmetrical around the center with P1 and P2 near it and C1 and C2 in further distance; P1P2=a, C1P1=C2P2=na, C1P2=C2P1=$(n+1)a$.

$$\left.\frac{\delta\varphi}{\delta\rho}\right|_{\mathrm{Schlum}} = \frac{4I}{\pi}\left\{\frac{z}{[4z^2+a^2]^{\frac{3}{2}}} - \frac{z}{[4z^2+((n+1)a)^2]^{\frac{3}{2}}}\right\}$$

Wenner array is an equidistant row of electrodes C1-P1-P2-C2 with a being the distance between the nearest electrodes.

$$\left.\frac{\delta\varphi}{\delta\rho}\right|_{\mathrm{Wen}} = \frac{4I}{\pi}\left\{\frac{z}{[4z^2+a^2]^{\frac{3}{2}}} - \frac{z}{[4z^2+(2a)^2]^{\frac{3}{2}}}\right\},$$

with maximum at $z = 0.32a$.
Dipole-Dipole array has C2 and C1 separated by distance a, P1 and P2 separated by the same distance a and these pairs separated by distance na.

$$\left.\frac{\delta\varphi}{\delta\rho}\right|_{\mathrm{d-d}} = \frac{2I}{\pi}\left\{\frac{z}{[4z^2+(na)^2]^{\frac{3}{2}}} + \frac{z}{[4z^2+((n+2)a)^2]^{\frac{3}{2}}} - \frac{2z}{[4z^2+((n+1)a)^2]^{\frac{3}{2}}}\right\}$$

Pole-Dipole array has the virtual current electrode C2 indefinitely far from the profile. Since contribution of every pair is reciprocally dependent on the distance between the electrodes, we can omit every pair with C2 in it. P1P2=a, C1P1=na. This sensitivity function, when normalized, is of the

same shape as in Schlumberger configuration; however with one electrode missing, the measured profile is much smaller.

$$\left.\frac{\delta\varphi}{\delta\rho}\right|_{\mathrm{p-d}} = \frac{2I}{\pi}\left\{\frac{z}{[4z^2+na^2]^{\frac{3}{2}}} - \frac{z}{[4z^2+((n+1)a)^2]^{\frac{3}{2}}}\right\}$$

Pole-Pole array has two electrodes in infinite distance, so its depth-sensitivity is the same as for the current-potential pair with C1P1=a.

$$\left.\frac{\delta\varphi}{\delta\rho}\right|_{\mathrm{p-p}} = \frac{2I}{\pi}\frac{z}{[4z^2+a^2]^{\frac{3}{2}}},$$

Maximum of this function gives the highest sensitivity in the depth of $0.35a$.
All sensitivity functions are illustrated for specific set of parametres in Chapter 1 of this brochure.